Assessing Future Changes of Climate and Drought over the South-Central United States Projected by the CMIP5 Models

Rong Fu, Nelun Fernando*, Lei Yin, Tong Ren, Ze Yang, Adam Bowerman, Robert E. Dickinson

Jackson School of Geosciences, The University of Texas at Austin

*University Corporation for Atmospheric Research, Postdocs Applying Climate Expertise (UCAR-PACE) Postdoctoral Fellowship Program

Abstract:

Nine climate models that participated in the Inter-governmental Panel for Climate Change (IPCC) Fifth Assessment Report (CMIP5) realistically capture the general patterns of seasonal cycle, the probability distributions of rainrate and surface daily maximum and minimum temperature (Tmax, Tmin), and the statistical distributions of the drought indices over the south-central United States (SC US). However, most of them have wet and cold biases in precipitation and Tmax, and underestimate non-rainy days and heavy to violent rainfall events and overestimate moderate rain. These biases are consistent with their underestimates of the latitudinal gradient of 500 hPa geopotential height in winter and spring, the strength and extent of the mid-tropospheric geopotential ridge, and the lower tropospheric westerly winds in summer. The former allows more frequent passages of synoptic disturbances during winter and spring, whereas the latter weakens the circulation pattern in favor of summer droughts. Although a few models can partially capture the Pacific-North American wave-train patterns, the models cannot fully capture the tele-connection patterns associated with El Niño-Southern Oscillation (ENSO) and its influence on rainfall anomalies over the SC US. Only CCSM4 reproduces the observed global SST warming mode and its relationship with an increase of summer rainfall over the SC US, and also out-performs other models in realistically representing most of the metrics used in our evaluation. Examination of multi-model ensemble mean and "the best performing model" (CCSM4) suggests that projection of drying for the SC US under the RCP4.5 is ambiguous, but under the RCP8.5 scenario it is robust.

1. Introduction

The worst single year drought over the SC US in 2011 and the worst drought in 60 years that a much large fraction of the US is experiencing in 2012 are vivid reminders of the vulnerability of our society to droughts. To improve drought resilience, regional decision makers need to know whether and how climate will change, especially whether the statistical characteristics of droughts and extreme surface temperature and rainfall will change, in the future. The climate projections by the CMIP5 modeling groups provide key information for regional decision makers. However, large inter-model discrepancies and apparent disagreement with observed changes during the past century over this region have largely prevented regional stakeholders from incorporating climate projections into their planning activities so far.

The climate community has done extensive research to assess future climate change, and the underlying mechanisms driving climate over the southwest and southeast US and the US Great Plain (e.g., Seager et al. 2007, Cook et al. 2008; Li et al. 2011) using the Coupled Model Intercomparison Project Phase-3 (CMIP3) model outputs. However, few studies have focused on future climate changes over the SC US. Consequently, regional stakeholders only have access to studies that primarily focus on the SW US and the Great Plains (e.g., Seager et al. 2006; Karl et al. 2009). Recently, several studies have assessed future climate changes over Texas (Mishra and Singh 2009; Jiang and Yang 2012). However, the reliability of climate projections for this region has not been investigated thoroughly.

Although drought has occurred frequently in recent years, mean annual rainfall over the SC US has been increasing over the last century (e.g., Dai et al. 2004; Trenberth et al. 2007). This increase of rainfall appears to be correlated with the global scale SST warming (Wang et al. 2010). By contrast, CMIP3 climate models have collectively projected a decrease of winter and

58 spring rainfall by 5% to 30% by the late 21st century (Karl et al. 2009, Jiang and Yang 2012).
59 Can climate models adequately represent the change of rainfall response over the SC US
60 resulting from global climate change? To clarify this question, we evaluate CMIP5 climate
61 models (Taylor et al., 2012). These models have included more comprehensive representations
62 of many climatic processes with finer spatial resolution and more ensemble members of
63 simulations for each model and scenario compared to the CMIP3 models. How realistically do
64 they represent current climate? What model qualities affect climate projections for the SC US?
65 The ultimate aim is to inform regional decision makers and so improve regional drought
66 resilience.

67 Whether model quality would have a significant impact on climate projections has been
68 debated. For example, Pierce et al. (2009) show that an ensemble mean, especially a multi-
69 model ensemble mean projection, can out-performs the best quality model because the former
70 allows cancellation of offsetting errors in the individual global models.

71 However, over some regions, models may share a similar bias that cannot be effectively
72 reduced by a multi-model ensemble averaging. Then, models realistically representing the
73 controlling mechanism of regional climate variability and its sensitivity to global climate change
74 could provide another constraint on uncertainty of the climate projections. In addition, a
75 demonstration of model quality in many cases is a prerequisite for policy makers to incorporating
76 climate projection into their decision making processes.

77 The selection of metrics can strongly influence the relevance of model evaluation for
78 improving climate projections. Past studies have focused on assessment of climatology, natural
79 variability and trends, important measures of the model creditability, but not providing
80 information about whether a model adequately captures regional climate sensitivity to

anthropogenic forced global climate change. For example, an evaluation of trend for the period of a few decades with a few climate model simulations can be strongly influenced by random internal variability, i.e., an agreement between a modeled and observed variable can be a random coincidence, rather than a demonstration of the capability of a model for prediction.

One way to evaluate regional climate sensitivity is to examine the relationship between regional climate change and the global warming trend, rather than a regional climate trend alone. Such a relationship can be evaluated by observations. This study develops such a relationship as a key metric in ranking the quality of climate models. It is used with other metrics that evaluate key large-scale circulation variables and their relationships with ENSO, AMO and global SST warming pattern, in order to evaluate projections of future climate by a multi-model ensemble and a "best performing model".

2. Description of Datasets, Models and Methodologies

2.1 Datasets:

We used the CPC US-Mexico daily gridded rainfall dataset (Higgins et al., 1996) over the domain 22.5°N-40°N and 110°W-90°W. It comprises an archival (from 1948-2004 at 1° resolution) and a real-time (2001 to present at 0.25° resolution) component that we combined to obtain a continuous time series from 1950-2005. These data are re-mapped to a 2.5° resolution to match the lowest resolution of the CMIP5 models. Daily Tmin and Tmax were obtained from the Global Historical Climatology Network (GHCN) dataset (Vose et al., 1992), and gridded to 2.5° resolution using the Weaver Analysis technique. In the absence of adequate long-term measurements of evapotranspiration (ET), we use the monthly ET provided by the North American Land Data Assimilation (NLDAS) of the Goddard Land Data Assimilation Data

104 System (GLDAS) (Rodell et al., 2004) obtained from http://mirador.gsfc.nasa.gov. The monthly
105 SSTs data are obtained from the Extended Reconstructed Sea Surface Temperature dataset
106 (ERSSTv3b, Smith et al., 2008) for the period 1901-2005, and the fields of 500 hPa geopotential
107 height (Z500), and zonal and meridional winds at 850 hPa (U850, V850) are obtained from the
108 National Center for Environmental Prediction (NCEP) reanalysis (Kalnay et al., 1996; Kistler et
109 al., 2001)
110
111 ***2.2 CMIP5 models and the simulations used in this study***
112 CMIP5 is organized by the World Climate Research Programme (WCRP) in order to
113 facilitate the IPCC AR5. It's model archives have been collected by the Program Climate Model
114 Diagnosis and Intercomparison (PCMDI). Over 20 modeling groups from all over the world
115 have participated in this project and conducted a variety of designed experiments (Taylor et al.,
116 2012). We selected the following models as described in Table 1. Except for GFDL-ESM2M
117 and GFDL-ESM2G, each model has more than three ensemble members for a specific
118 experiment or scenario. We use ensemble averages for each model to improve the signal-to-
119 noise ratio of the modeled fields and to give an equal weight to each model in the multi-model
120 ensemble mean. GFDL-ESM2M and GFDL-ESM2G each only provide one simulation per
121 experiment. Their results can be strongly influenced by random noisy. The historical
122 simulations are driven by all the natural and anthropogenic forcings and are mostly from 1850 to
123 2005. We used the time period of 1950-2005 for model evaluation when observations are of
124 adequate quality, and the period of 1979-2005 as the reference to compare with the projected
125 climate for the period of 2071-2100 derived using the Representative Concentration Pathways
126 (RCPs, Meehl and Hibbard, 2007a; Hibbard et al, 2007; Moss et al, 2010) scenarios of RCP4.5

and RCP8.5 that assume that the radiative forcing will be stabilized at 4.5 Wm^{-2} and 8.5 Wm^{-2}, respectively, after 2100.

2.3 Metrics of model evaluation

Gleckler et al. (2008) and Pierce et al. (2009) have recommended metrics for a comprehensive evaluation of the general performance of global climate models. However, to focus on assessment of droughts and their controlling processes over the SC US, we select a subset of the climate variables from the recommended metrics that are highly relevant to the processes that control the development and occurrence of droughts.

Previous studies have shown that a persistent high pressure system and middle tropospheric ridge, and dry land surface are key conditions for summer drought over SC US (e.g., Hong and Kalney 2002, Myoung and Nielsen-Gammon 2010). Strong westerly winds advect dry and warm air from the Mexican Plateau and Rockies to the SC US and enhance cap-inversions in the lower troposphere. Lower tropospheric southerly winds bring warm and humid air from the Gulf of Mexico, creating a favorable condition for rainfall. Dry conditions during late spring sets the stage for summer droughts. Prolonged droughts from winter to summer often lead to extreme droughts. These conditions also favor the occurrence of extreme summer surface temperature, because of strong inverse correlation between high surface temperature and dry land surface in this region (Madden and Williams 1978).

Drought over the SC US is initiated by La Niñas in boreal winter, and could be intensified by a positive phase of the Atlantic Multi-decadal Oscillation (AMO, McCabe et al. 2004; Hu and Feng, 2008, Mo et al. 2009, Kushnir et al. 2011, Nigam et al. 2011). However, ENSO and AMO are random modes of internal variability. Thus, we focus on the realism of

150 ENSO teleconnection pattern and the relationship between regional rainfall anomalies and ENSO
151 and AMO. We separately evaluate the tele-connection patterns for the eastern Pacific warming
152 (EPW) Niño and the central Pacific warming (CPW) Niño, respectively, because they have
153 different impacts on US climate (Mo 2009), and the occurrence of these two types of ENSO may
154 be influenced by anthropogenic forced warming (Yeh et al. 2009). A couple of centuries could
155 be needed to adequately assess ENSO and AMO variability (Wittengberg 2009; Stevenson
156 2012). Thus, significance of our evaluation on how such natural climate variability influences
157 the SC US climate is somewhat limited by lengths of climate records and historical simulations.
158 In addition, Wang et al. (2010) have suggested a statistical correction between an
159 increase of summer rainfall over SC US and global increase of SSTs. Because this global
160 increase of SST is attributable to anthropogenic forcing (e.g., Barnett et al. 2001), we will
161 evaluate this relationship as an indicator of regional rainfall sensitivity to forced global climate
162 change.
163 The multi-model ensemble mean may not be more reliable than the "best performing
164 model" when a majority of the models share common biases. However, "best performing
165 models" are limited by insufficient samples and statistical representation of the variability of the
166 climate system. Thus, we evaluate historical simulations of both multi-model ensemble means
167 and best performing models, and assessing the robustness of the climate projections based on the
168 consistency between them.
169
170 ***2.4 Analysis methods***
171 The SC US domain in our analysis includes Texas and portions of New Mexico,
172 Oklahoma, Louisiana, Arkansas, Kansas and Missouri (Fig. 1). Because severe to extreme

drought over the SC US are caused by persistent water deficit over two to three seasons, we evaluate the modeled 6- and 9-monthly Standardized Precipitation Index (SPI6 and SPI9) calculated (McKee et al. 1993) using monthly mean precipitation derived from the US-Mexico daily gridded precipitation dataset. Because we are interested in the changes of SPI6 and SPI9 relative to present-day climatology, we normalize the rcp4.5 and rcp8.5 precipitation data for 2070-2099 with the mean and standard deviation of precipitation from base period of 1970-1999. The normalization is carried out prior to calculating SPI6 and SPI9 using projected precipitation.

Follow Schubert et al. (2009), the global SST warming mode is represented by the leading mode of the Rotated Empirical Orthogonal Function (REOF, Barnston and Livezey, 1987; O'Lenic and Livezey, 1988) of the annual and summer (JJA) global sea surface temperature (SST) anomalies. The Niño3 and Niño4 are computed as the domain averaged SST anomalies over the region of 150°W-90°W and 5°N-5°S, and of 160°E-150°W and 5°N-5°S, respectively. The Atlantic Multidecadal Oscillation (AMO) is described as the area weighted average of SSTA over the northern Atlantic, basically from 0 to 70°N (Endfield et al. 2001). The detailed calculation procedure is found on NOAA/ESRL website: http://www.esrl.noaa.gov/psd/data/timeseries/AMO/. Statistical significant tests of correlation coefficients are determined by the Student-T test.

3. Evaluation of Historical Simulations

3.1 Regional climatology and variability

a. Surface conditions

Figure 2 compares the seasonal cycles of surface air Tmax, Tmin and surface air specific humidity (q) simulated by the 9 CMIP5 models to those derived from the GHCN data, NOAA

196 CPC US-Mexico daily gridded datasets and NCEP CDAS-1. The models capture the seasonal
197 variations of Tmax and Tmin over the SC US. However, the models appear to consistently
198 underestimate Tmax values by as much as 5-7 °C during winter, and spring and fall (Fig. 2a). In
199 summer, Tmax values in one third of the models (HadGEM2-CC, CCSM4 and MIROC5) agree
200 with observations, but they are underestimated in two-thirds of the models by as much as 5 °C.
201 The multi-model ensemble mean shows a similar patterns and biases as those of individual
202 models.

203 Tmin values in most of the models and multi-model ensemble mean agree well with that
204 observed (Fig. 2b). MIROC, CCSM4 overestimate Tmin by 1-2 °C in summer and fall, whereas
205 HadGEM2, IPSL over underestimate Tmin by 3 °C in winter. The modeled surface air specific
206 humidity agrees well with the observation, except for HadGEM2-CC and IPSL (Fig. 2c).

207 Figure 3 compares the modeled seasonal cycles of precipitation (P), evapotranspiration
208 (ET) and P-ET to those observed. Observations show that rainrate over the SC US is generally
209 higher than 2 mm/day during April to October and below 1.5 mm/day from October to March.
210 Peak rainfall occurs in May, about 2.5 mm/day, and annual minimum occurs in January, ,about
211 1.5 mm/day. The CCSM4 and MPI best capture this seasonal pattern. HadGEM2, GFDL-
212 ESM2M and MRI show a spurious mid-summer dry period, leading to a semi-annual cycle
213 peaking between spring and early fall. IPSL shows a short summer peak of rainfall with very dry
214 spring and fall seasons. Except for IPSL, models consistently overestimate rainfall by 0.5 to 1
215 mm/day with large inter-model discrepancies during spring and summer seasons.

216 Figure 3b shows that models generally capture the seasonal cycle of ET shown by
217 NLDAS, although two-thirds of them underestimate the values of ET. The GISS model
218 overestimates ET by as much as 250%, whereas IPSL and CCSM4 underestimate ET by nearly

219 30% in summer. The high bias of multi-model ensemble mean is largely due to strong bias of
220 GISS model.

221 P- ET represents the net water flux available to the surface, thus it has strong influence on
222 meteorological drought and wet surface and flood. Figure 3c shows that P-ET estimated by
223 observation and NLDAS is positive during fall, winter and spring (September to March) and
224 peaks in winter at the rate of about 1 mm/day, and negative during summer (June-August) at
225 about -1 mm/day. Most of the models capture this seasonal pattern of P-ET, but underestimate
226 the magnitude of surface water loss (negative P-ET). The GISS model substantially
227 overestimates the magnitude of surface water loss due to its strong overestimate of ET (Fig. 3b),
228 whereas CCSM4 does not capture the observed negative P-ET in summer. The multi-model
229 ensemble mean shows good agreement with that observed due to a balance between
230 overestimated and underestimated P-ET values among different models.

231 The probability distributions (PD) of Tmax, Tmin and rainrate are important in
232 determining statistical distributions of extreme climatic events. Fig. 4a shows that Tmax has a
233 distribution over the SC US that ranges between 23 °C – 33°C or about 72 °F – 90 °F skewed
234 toward warmer Tmax values. The models capture the general shape of the PD. However, they
235 consistently underestimate the probability of hot to extreme Tmax (33°C – 53°C, or about 90 °F
236 – 126 °F), and overestimate probability of colder Tmax (-18 °C – 12°C, or 0 °F – 55 °F), except
237 for MIROC5. The majority of the models and multi-model ensemble mean also capture the
238 general pattern of PD of Tmin, although they consistently underestimate probability of cooler
239 Tmin (-13 °C – -3°C or 10 °F – 27 °F). MIROC5 and CCSM4 also substantially overestimate the
240 probability of warmer Tmin (17 °C – 27 °C or 63 °F – 81 °F).

241 Fig. 4c shows that the models consistently underestimate of probability of non-rainy days
242 and violent rainy events (>50 mm/day), and overestimate moderate rainy events (2.5-10
243 mm/day). These biases contribute to the overestimate of climatological rainfall (Fig. 3).
244 HadGEM2-CC and MPI provide the most realistic PD of rainrate.
245 How well can models simulate drought and persistent anomalous wet periods? Figure 5
246 shows that the models well capture the median, 25% and 75% values of the SPI6 and SPI9,
247 respectively, between observation and historical simulations for the period of 1951-2005.
248 However, the comparison of outliners suggests that most of the models underestimate dry
249 outliners, or extreme to exceptional droughts (-4<SPI6, SPI9<-3).
250
251 ***b. Atmospheric circulation***
252 To investigate the underlying causes of the biases in regional surface climate conditions,
253 this section evaluates modeled atmospheric circulation patterns in this section. Figure 6 shows
254 that, except for CCSM4, all other models underestimate the latitudinal gradient of Z500 in
255 winter, spring and fall compared to observations. Such a bias implies weak jet strength and more
256 frequent or/and stronger synoptic disturbances from higher latitudes can reach SC US. Such a
257 bias would contribute to strong cold biases in Tmax and Tmin and an overestimation of rainfall
258 in winter and spring. CCSM4 has the least cold and wet biases during winter and spring, which
259 is consistent with its stronger latitudinal gradient of Z500 than other models.
260 During summer, the models generally underestimate the strength and area of the 500 hPa
261 ridge, except for CCSM4 and MIROC5. A weak 500 hPa ridge could contribute to an
262 overestimating of rainfall, and favoring lower Tmax in these models. Lack of such a bias in

263 CCSM4 and MIROC5 presumably explains the higher summer Tmax in these two models than
264 the other models.

265 In figure 7, we compare modeled U850 and V850 over the US with that observed.
266 Modeled U850 over the SC US is more realistic during winter and fall (Fig. 7a). The models
267 underestimate westerly U850 in spring, except for CCSM4, MPI and IPSL. Because strong
268 westerly U850 during spring can trigger summer drought (Hong and Kalney 2002, Fernando et
269 al. 2012), its weak bias would likely contribute to spring wet anomalies in the models.

270 Figure 8 shows that all the models underestimate southerly V850 in winter. During
271 spring, summer and fall, they, except for HadGEM2, also consistently underestimate southerly
272 V850 over the SC US except for HadGEM2. Because southerly V850 dominates the transport of
273 warm and moisture from Gulf of Mexico to SC US, its underestimate probably contributes to a
274 cold bias in Tmax and Tmin in spring and low biases in surface air q. However, it's potential
275 impact on rainfall is presumably compensated by biases in Z500 and U850.

276

277 ***3.2 Relationship with interannual and decadal climate variability modes***

278 Whether or not climate models can adequately represent the connections between
279 regional climate anomalies and its oceanic forcing is central in determining the frequency and
280 intensity of droughts and probability of extreme temperatures and rainfall, and is investigated in
281 this section. Figure 9 compares the modeled and observed correlation coefficients for the areal
282 averaged rainfall anomalies over the SC US with the EPW Niño index (Niño3) and the CWP
283 Niño index (Niño4), respectively. Observed rainfall over the SC US is significantly positively
284 (negatively) correlated with El Niño (La Niña), occurs only in winter (DJF). This seasonal
285 dependence of correlation is only captured by the GISS-E2R. The other models either capture

this relationship in winter, but also exaggerate its seasonal persistence during other seasons (GFDL-ESM2M, GFDL-ESM2G, MIROC5, IPSL), or show spurious correlation between the SC US rainfall and ENSO in spring, summer for fall (CCSM4, HadGEM2-CC and MPI-ESM), or do not show any relationship between the SC US rainfall anomalies and ENSO (MRI-CGCM3).

The influence of ENSO on SC rainfall anomalies is determined by the ENSO teleconnection pattern. Figure 10 shows the spatial pattern of the correlation between the Z500 anomalies and Niño3 index during winter (DJF) when regional rainfall anomalies are significantly correlated with ENSO indices. None of the models appear to capture the overall spatial pattern of the correlation for the period of 1979-2005. CCSM4, GFDL-ESM2G, GFDL-ESM2M partially capture the dipole of strengthened North American High and a weakened Aleutian Low.

Figure 11 shows that the strengthening of North American High related to the CPW Niño (Niño4) is not as strong as that related to the EPW Niño (Niño4). Again, none of the models can entirely capture the spatial pattern of the correlation between Z500 anomalies and Niño3. However, CCSM4, GFDL-ESM2G, GFDL-ESM2M and MRI partially capture the dipole that strengthens the North American High and deepens the Aleutian Low, although the positive anomalous Z500 center over North America is biased too southward compared to that suggested by NCEP reanalysis.

We have also evaluated the standard deviations of the Niño3 and Niño4 indices normalized by those derived from observation. The results suggest that the normalized standard deviations of modeled Niño indices in CCSM4, GFDL-ESE2M, GFDL-ESM2G, HadGEM2 and MIROC5 are close to one. Thus, the magnitudes of the ENSO variability in of Niño3 and Niño4

309 indices are comparable to those observed. The results also show that the variability of Niño3 and
310 Niño4 indices in GISS-E2-R, IPSL, MPI and MRI are only about 40% or less than those
311 observed.
312 The relationship between AMO index and the SC US rainfall anomalies is evaluated in
313 Figure 12. Despite the suggested AMO influence on North American rainfall in general, no
314 significant correlation is detected observationally, nor suggested by most of the models over SC
315 US, except for CCSM4 and IPSL. These two models suggest an unrealistic correlation between
316 the SC US rainfall and AMO during spring and winter, respectively. The lack of significant
317 correlation between AMO and the SC US rainfall is consistent with previous observational
318 studies that suggest that AMO influences North American rainfall primarily through its
319 modulation of ENSO influence (e.g., Hu and Feng 2008).
320 Although none of the models can satisfactorily capture the ENSO tele-connection
321 patterns and its influence on the SC US rainfall anomalies, CCSM4, GFDL-ESM2G, GFDL-
322 ESM2M appear to out-perform other models. However, CCSM4 overestimates the connection
323 between the SC US rainfall and AMO.
324
325 ***3.3 Relationship with global SST warming mode***
326 How well can CMIP5 models represent the responses of the SC US climate and extremes
327 to an increase of global surface temperature? To explore this question, we first evaluate the
328 spatial pattern of the REOF mode of SST anomalies that represents the global increase of SST
329 for JJA, the season when the ENSO influence on SST is relatively low (Fig. 13). As the leading
330 REOF mode of the observed SST anomalies (Schubert et al. 2009), it shows warming over most
331 of the global ocean, except for over high-latitude North Atlantic and northwestern Pacific, and

equatorial eastern pacific. The spatial pattern of this global SST warming mode is best captured by GFDL-ESM2G and GISS as their leading REOF mode. CCSM4 and MPI also capture the general pattern of the warming mode, although they either overestimate the cooling over North Pacific or over the equatorial Pacific. In HadGEM2-CC, MIROC5 and GFDL-ESM2M models, ENSO emerges as the leading REOF mode of SST anomalies. The global SST warming mode emerges as the second or even the third leading REOF mode, suggesting these models underestimate the influence of the global SST warming on SST variation.

The principle component of the leading REOF mode (PC1) of the observed SST anomalies suggests a steady warming during 1950-1990, then it has leveled off since 2000. The modeled PC1s of SSTs suggest a warming trend since 1970s or 1980s, except for HadGEM2-CC and MRI-CGCM3. This difference in temporal behavior of the PC1 maybe in part due to possible modulation of the global SST warming mode by natural decadal variability and lack of it in the modeled PC1s. The PCs of the global SST warming mode in HadGEM2-CC and MRI-CGCM3 models show spurious changes during early 20th century, suggesting that the SST warming is either inadequately modeled or not robust enough for our REOF reanalysis to capture it.

Because droughts and summer extreme temperature over the SC US are mostly influenced by rainfall, we evaluate the linear regression between the SC US rainfall and the PC of the global SST warming mode for both annual means and JJA season (Fig. 14) to explore impact of the latter on droughts and extreme temperatures over the SC US. No models could capture the positive correlation between the annual mean rainfall anomalies of SC US and the PC1 of global annual mean SST anomalies. However, in the summer (JJA) season, CCSM4 and GFDL-ESM2M both capture the significant increase of the SC US rainfall associated with

355 warming of global SSTs as observed, although GFDL-ESM2M may overestimate the rate of
356 regional rainfall change associated with the global SST warming. GISS-E2R and MIROC5 show
357 a significant decrease of the SC US rainfall with the global SST warming, opposite from that
358 observed. The other six models do not show any significant change associated with the global
359 SST warming.

360 In short, figures 13 and 14 suggest that CCSM4 and GFDL-ESM2M capture both the
361 observed global SST warming mode and its link with the SC US rainfall, whereas other models
362 are unable to adequately capture either the global SST warming mode or its relationship with the
363 SC US rainfall change.

364

365 ***3.4 Ranking of model performance***

366 For assessing overall performance and its implications for the models in projecting
367 climate change over the SC US, we broadly rank the models according to the metrics and
368 rationales described in Section 3.3. Models that realistically capture the patterns of the spatial or
369 temporal variability, changes and correlation for a selected climate variable are ranked as the top
370 performing or Class-1 models for that variable. The models that partially agree with the
371 observations, including the signs of correlation or changes, are ranked as average performing
372 (Class-2) models. Models that show no resemblance to observations, e.g., showing wrong signs
373 of correlation between regional climate responses to external forcings, are ranked as the under-
374 performing (Class-3) models. Climate projections are based on the response of the regional
375 climate to warming induced by an increase of global radiative forcing, and anticipated dominant
376 influence by changes of radiative forcing over natural climate variability on climate conditions at
377 the end of 21st century. Thus, we assign more weight to a model's performance in seasonal

cycles and relationship with the global SST warming mode than to internal natural variability such as change associated with ENSO.

Following the above guidelines, the models' performance in representing the SC US regional climate is ranked in Table 2. The CCSM4 is the only model that is ranked in either category 1 or 2 in representing the global SST warming mode (GW_{sst}) and its relationship with the SC US regional rainfall change (α_{GW}). Thus, it outperforms other models, whose average is 2.0 or higher for these variables, in this key criterion for assessing reliability of the climate projection. CCSM4, MPI and MRI have seasonal cycle average ranking below 2.0 but more for the natural variability ranking. The latter requires more observational and model data than available to establish statistical significance for its variables (Wittengberg 2009; Deser et al. 2012).

4. Climate Projections for the Late 21st Century

To assess climate change over the SC US in the future, we evaluate projected regional climate conditions for the period of 2071-2100 (referred to as the late 21st century) under the RCP4.5 and RCP8.5 scenario, respectively, and compare them to the historical simulations for the period of 1979-2005 (referred to as the recent past) for each model. Ensemble mean of individual simulations for each model and each scenario are used for assessing the changes, except for in figures 15 and 16 to avoid the impact of sampling difference on our comparison between different models. The periods of comparison are based on the recommendation of NOAA MAPP CMIP5 task force for publication in this special issue. The projections of multi-model ensemble means and those of the best performing model will be compared in our discussion. Because of the model biases as shown in Section 3, we will focus more on changes

401 of the climate conditions than on absolute values. For brevity we do not show the analysis of
402 projected circulation change.
403
404 ***4.1 Projected changes in surface climate conditions***
405 Figure 15 shows the projected Tmax distributions for each model over the SC US by the
406 late 21st century compared to that in the recent past. Under the RCP4.5 scenario, the individual
407 models and the multi-model ensemble mean consistently project a more skewed PD toward
408 warm temperatures, except for MIRCO5. The occurrence of warm temperatures, ranging from
409 32˚C to 42˚C (89.6˚F to 107.6˚F), increases by 25% to 50% relative to those of recent past. The
410 occurrence of Tmax cooler than 3˚C decreases. The occurrence of Tmax with medium values
411 (3˚-22˚C) will only change slightly. The peak of the temperature distribution will remain at 22˚C
412 - 32˚C, the same as that in the recent past. MIROC5, on the other hand, projects a shift of peak
413 Tmax distribution to 32˚C-42˚C (90˚ – 108˚F) in the late 21st century.
414 Under the RCP8.5, the projected change of PD patterns are similar to those of RCP4.5
415 scenario, but warmer Tmax, ranging from 32˚C to 42˚C, will increase by 50%-100% relative to
416 their occurrence in the recent past. Although the peak of Tmax distribution will be the same as
417 projected by the majority of the models, more models (HadGEM2, MPI, MIROC5) project a
418 shift of the peak Tmax distribution to 32˚C-42˚C. Such projections suggest that the summer
419 extreme temperatures during the late 20th century will become normal in future. For both
420 emission scenarios, the projected changes of Tmax distribution are very similar between the
421 multi-model ensemble mean and the best performing model.
422 The project changes of Tmin distribution is shown in Fig. 16. For both emission
423 scenarios, the models consistently project more occurrences of Tmin that exceed 22˚C and a

424 decrease of Tmin below -3˚C in future. The occurrence of medium Tmin will not change for
425 more than a few percentages. Two-thirds of the models project a shift of peak Tmin distribution
426 to 17˚C -27˚C by late 21st century under both the RCP scenarios, from 7˚C -17˚C. These models
427 also project an increase of the occurrence of Tmin warmer than 27˚C (80.6F) by several folds
428 under the RCP8.5 scenario.

429 Figure 17 shows projected changes of distribution of rainfall intensity in the late 21st
430 century. The majority of the models and multi-model ensemble mean suggest an increase of
431 non-rainy and light rainy days, and a decrease of light to moderate rainy days (0.25-10 mm/day)
432 for both emission scenarios. The changes of rainrate distribution are more than twice as strong
433 for the RCP8.5 scenario as for the RCP4.5 scenario. The "best performing model" (CCSM4), on
434 the other hand, projects little change in rainrate distribution under the RCP4.5 scenario. It
435 projects a slight decrease of non-rainy and light rainy events and an increase of heavy rainfall
436 days (10-50 mm/day).

437 What could cause a preferential increase of warm to hot, and extreme Tmax? Because
438 these high Tmax values occur with dry and hot land surface conditions during warm seasons
439 (e.g., Madden and Williams 1978), we evaluate changes of precipitation, ET, and net surface
440 water flux in different future seasons in Figure 18. HadGEM2 and MPI are not included in this
441 figure because they did not provide projections of ET. The projected changes are noisy with
442 large inter-model discrepancies under both emission scenarios. Under the RCP4.5 scenario, the
443 multi-model ensemble mean shows weak increase of P and ET in winter and spring. CCSM4
444 also projects similar changes of P and ET, but with a stronger increase of rainfall during
445 February and June, and a weaker decrease of rainfall in late summer, compared to the multi-
446 model ensemble projection. The multi-model ensemble projection shows a decrease of P-ET or

447 an increase of surface water loss to the atmosphere from spring to fall, thus much drier surface
448 conditions. In contrast, CCSM4 projects a weak increase of P-ET all year round as a result of its
449 stronger increase of rainfall, and hence more supply of surface water and runoff. Because
450 CCSM4 is the only model (here evaluated) that is capable of reproducing the observed increase
451 of rainfall of the SC US with the increase of global SST in the recent past, its projected increase
452 of P-ET may be a result of such capability. The discrepancy between the projections by multi-
453 model ensemble mean and best performing model suggests that the projected change is not
454 robust under the lower emission scenario.

455 Under the RCP8.5 scenario, the patterns of P, ET, P-ET changes are similar to those of
456 RCP4.5, but magnitudes of the changes increase. Both multi-model ensemble projection and
457 CCSM4 project a decrease of P-ET and an increase of surface water loss during spring, summer
458 and fall, resultant from a faster increase of ET than the increase of P and also from reduced gap
459 of P changes between the multi-model ensemble mean and CCSM projections. Thus, the
460 projected drying of land surface over SC US appears to be robust under this high emission
461 scenario. The projected increases of surface water loss during spring, summer and fall imply a
462 strong increase of dry spells. These changes can contribute to disproportionally large increase of
463 warm and hot Tmax as shown in Fig. 15.

464 How will drought and prolonged wet anomalies change in future? Figure 19 compares
465 the medium, 25% and 75% values of the SPI6 between the historical simulations, the RCP4.5
466 and RCP8.5 scenarios, respectively. To gain a prospective about changes from the recent past,
467 we modified the SPI calculation by using projected monthly rainfall subtracted from the
468 historical climatological seasonal cycle of rainfall to obtain cumulative rainfall anomalies, which
469 are then normalized by historical rainfall variability. Figure 19 shows a lack of consistency in

470 the projected changes of the SPI6 distribution. Except for CCSM4, the SPI6 projected by all
471 other models does not show changes of median values, but rather more than half of the models
472 (GFDL-ESM2G, GFDL-ESM2M, ISPL, MIROC5 and MPI) project a greater spread of SPI6
473 values, implying an increase of stronger droughts and persistent wet anomalies, in the late 21st
474 century. The multi-model ensemble mean shows the changes of SPI6 similar to that of most
475 models, but with a much reduced range of variability due to its averaging across models. On the
476 other hand, the "best performing model" (CCSM4) projects a negative shift of the median, 25%
477 and 75% of SPI6, suggesting more frequent and intense droughts in future. The negative shift of
478 the median SPI6 is stronger for the RCP8.5. The projected changes of SPI9 distributions are
479 similar to those of SPI6 (not shown).
480
481 **5. Conclusions and Discussion**
482 We have evaluated the performance of nine selected CMIP5 models in representing SC
483 US regional surface climate, its variability and changes, the key large-scale circulation patterns,
484 and their links to ENSO, AMO and the global scale SST warming mode, as a basis to assess the
485 fidelity of these models for climate projections over this region. A novel aspect of this
486 evaluation is its focus on the sensitivity of the regional climate response to the global scale
487 natural climate variability and change and the key circulation patterns that control the regional
488 droughts.
489 The evaluation suggests that the models generally adequately reproduce the observed
490 patterns of the seasonal cycles and the probability distributions of the surface temperature,
491 humidity and rainfall. However, the majority underestimates Tmax and q and overestimate Tmin
492 and P, especially during spring and early summer. The excessive rainfall is due to an

493 underestimate of non-rainy and light rainy days (<0.25 mm/day) and an overestimate of
494 moderate rainy days (0.25-10 mm/day). These models also consistently underestimate the
495 occurrence of days with heavy to violent rainfall events (>10 mm/day). Underestimates of the
496 latitudinal gradient of the mid-tropospheric (500 hPa) geopotential height in winter and spring,
497 the strength and area of the mid-tropospheric high, and westerly winds in the lower troposphere
498 probably all contribute to the surface wet and cool biases over the SC US.
499 The models appear to reproduce the values of median, 25% and 75% levels of SPI6 and
500 SPI9 values, despite their wet biases in rainfall climatology and inadequate links between SC US
501 rainfall, ENSO and AMO indices in the majority of the models. The majority of the models
502 appear to underestimate the occurrence of extreme to exceptional droughts. However, such
503 uncertainty could be artifact of insufficient samples available for the 55-year analysis period.
504 Only a few models (CCSM4, GFDL-ESM2G and GFDL-ESM2M) partially capture the tele-
505 connection pattern associated with the EPW (Niño3) and CPW Niño (Niño4) index, respectively.
506 However, these models tend to overestimate persistence of the ENSO influence on SC US
507 rainfall anomalies, and are unable to capture the seasonality of such influences. CCSM4 and
508 IPSL overestimate the correlation between SC US regional rainfall anomalies and AMO. Such
509 uncertainties highlight the challenge of modeling the impact of ENSO on regional rainfall in
510 global climate models.
511 Several models (CCSM4, GFDL-ESM2G, GISS, and MPI) appear to realistically capture
512 the global SST warming mode, as represented by the leading mode of the Rotated Empirical
513 Orthogonal Function (REOF) of the global SST anomalies. However, only CCSM4 simulates its
514 relationship with an increase of rainfall over the SC US. Inadequate representation of the
515 modeled rainfall response to the increase of global SSTs by the majority of the models raises a

question as to whether the multi-model ensemble projections are more or less reliable than the single "best performing model" for projecting the future drought and extreme temperatures over the SC US.

Overall, CCSM4 outperforms the other models in representing the relationship between SC US rainfall and the global SST warming mode, seasonal cycles of large-scale atmospheric circulation patterns. CCSM4 is also one of the few models that partially capture the tele-connection pattern associated with ENSO and the relationships between the SC US rainfall anomalies and ENSO. In addition to uncertainty of the models' physics, the apparent poor performance of the ENSO tele-connection patterns could be in part due to insufficient sampling of ENSO within our short analysis period (Wittengberg 2009; Stevenson et al. 2012).

Ensemble projections by the RCP4.5 and RCP8.5 experiments for the period of 2071-2100 are compared to those simulated by the historical simulations for the period of 1979-2005, to assess future changes over the SC US. Because the majority of the models share some common biases, we compare the multi-model ensemble projections with that of "best performing model" (CCSM4) to assess the robustness of the projections. Both multi-model ensemble mean and CCSM4 consistently project that a) the occurrence of Tmax ranging from 32˚ to 42˚C (~90˚ F to 108 ˚F) will increase by 25% to 50% in future relative to their occurrence in recent past for the RCP4.5 scenario, and their frequency of occurrence will increase 50%-100% for the RCP8.5 scenario. The occurrence of colder Tmax (<3˚C) will decrease. The distribution of Tmax will be skewed toward warmer temperature, but the peak will remain the same. b) The peak of the Tmin distribution will shift by 10˚C (18˚F) to 17˚C - 27˚C (63˚F -81˚F). The occurrence of below freezing Tmin will decrease under the RCP4.5 scenario. Under the high emission RCP8.5

538 scenario, the occurrence of Tmin exceeding 27˚C (80.6 F) could increase several times relative to
539 that in recent past.
540 There are large discrepancies in projected changes of distribution of rainrate, P, ET and
541 P-ET between individual models, the multi-model ensemble mean and the best performing
542 model. Under the RCP4.5 scenario, the majority of the models and multi-model ensemble mean
543 project a future increase of non-rainy and light rainy days (0-0.25 mm/day) and a decrease of
544 light to moderate rainfall (0.25-10 mm/day), whereas CCSM4 projects little change in the rain
545 rate distribution. Multi-models ensemble projections suggest a weak increase of P-ET winter,
546 spring and fall and a decrease of P-ET in summer. In contrast, CCSM4 projects an increase of P-
547 ET in winter, spring, early summer and fall, and a small decrease of P-ET in late summer. Most
548 models project a wider spread of SPI6 and SPI9 or increased intensity of both droughts and
549 persistent wet periods, without a clear shift of the medium values for SPI6 and SPI9. CCSM4, on
550 the other hand, shows a negative shift of SPI6 and SPI9 medium values without an increase in
551 their spread.
552 Under the RCP8.5 scenario, the majority of the models and multi-model ensemble
553 projections suggest a stronger change of rainrate distribution than those of RCP4.5 but without
554 systematic changes of SPI6 and SPI9 distributions. CCSM4, on the other hand, shows a weak
555 decrease of non-rainy and light-rainy days and an increase of heavy rainfall (10-50 mm/day), but
556 a more negative shift of median SPI6 and SPI9 values from those of RCP4.5.
557 The patterns of the changes of P, ET and P-ET are similar to those of RCP4.5, but
558 magnitudes of the changes increase. Both multi-model ensemble projection and CCSM4 project
559 a decrease of P-ET and an increase of surface water loss during spring, summer and fall, a
560 consequence of their stronger increase of ET and summer P in both the multi-model ensemble

561 mean and CCSM projections. Thus, the projected drying of land surface over SC US appears to
562 be robust for this high emission scenario.
563 Our assessment of the climate projections by the CMIP5 models suggest that, while a
564 climatic shift of the hydrological cycle over SC US for weak global warming is questionable, the
565 projections for an climatic drying over this region under a growing emission scenario (RCP8.5)
566 seems to be robust. Thus, future climatic drying over SC US may be rather sensitive to future
567 emission policies.
568 One of the main limitations of our assessment is its insufficient representation of the
569 statistical distributions of the climate variables we evaluate due to both short duration of
570 available observations, model simulations and limited ensemble members of simulations. For
571 the regions such as SC US, multi-model ensembles cannot effectively remove common biases
572 among the majority of the models. However, a large number of ensemble simulations by the
573 "best performing models" could provide an alternative and complementary approach to reduce
574 the uncertainties of the climate projections.
575
576 **Acknowledgement:**
577 We acknowledge the World Climate Research Programme's Working Group on Coupled
578 Modelling, Which is responsible for the Coupled Model Intercomparison Project (CMIP). We
579 thank the climate modeling groups for producing and making their model outputs available, the
580 US Department of Energy's Program for Climate Modeling Diagnosis and Intercomparison
581 provides coordinating support and let development of software infrastructure in partnership with
582 the Global Organization for Earth System Science Portals. This work is supported by the NOAA
583 Climate Program Office Modeling, Analysis, Prediction and Projection (MAPP) Program

584 through Grant NA10OAAR4310157; the Postdocs Applying Climate Expertise (PACE)
585 Postdoctoral Fellowship Program, partially funded by the NOAA Climate Program Office and
586 administered by the University Corporation for Atmospheric Research (UCAR) Visiting
587 Scientist Programs (VSP); the National Science Foundation (NSF) AGS-0937400; and the
588 Jackson School of Geosciences.
589
590

Reference:

Barnett, T. P., D. W. Pierce, R. Schnur, 2001:Detection of Anthropogenic Climate Change in the World's Oceans, Science 292, 270 (2001).

Barnston, A. G., and R. E. Livezey (1987), Classification, seasonality and persistence of low-frequency atmospheric circulation patterns, *Monthly Weather Review*, *115*, 1083-1126.

Clement, A. C., R. Burgman, and J. R. Norris, 2009: Observational and Model Evidence for Positive Low-Level Cloud Feedback. *Science*, 325, 460-464.

Cook, K. H., E. K. Vizy, Z. S. Launer, and C. M. Patricola, 2008: Springtime Intensification of the Great Plains Low-Level Jet and Midwest Precipitation in GCM Simulations of the Twenty-First Century. *Journal of Climate*, 21, 6321-6340.

Dai, A., K. E. Trenberth, and T. T. Qian, 2004: A global dataset of Palmer Drought Severity Index for 1870-2002: Relationship with soil moisture and effects of surface warming. *Journal of Hydrometeorology*, 5, 1117-1130.

Deser, C., A. Phillips, V. Bourdette, and H. Y. Teng, 2012: Uncertainty in climate change projections: the role of internal variability. *Climate Dynamics*, 38, 527-546.

Enfield, D.B., A.M. Mestas-Nuñez, and P.J. Trimble, 2001: The Atlantic Multidecadal Oscillation and its relationship to rainfall and river flows in the continental U.S. *Geophys. Res. Lett*., 28, 2077-2080.

Gleckler, P. J., K. E. Taylor, and C. Doutriaux, 2008: Performance metrics for climate models. *Journal of Geophysical Research*, 113, D06104.

Hibbard, K. A., G. A. Meehl, P. Cox, and P. Friedlingstein, 2007: A strategy for climate change stabilization experiments. *EOS*, 88, 217, 219, 221.

Higgins, R. W. J., J.E., Yao, Y-P, 1996: A Gridded Hourly Precipitation Data Base for the United States (1963-1993). U. S. D. O. C. *NCEP/Climate Prediction Center ATLAS No. 1, National Oceanic and Atmospheric Administration, National Weather Service*, Ed.

Hong. S. Y. and E. Kalney, 2002: The 1998 Oklahoma-Texas drought: Mechanistic experiments with NCEP global and regional models, *J. Climate*, 15, 945-963.

Hu, Q., and S. Feng, 2008: Variation of the North American Summer Monsoon Regimes and the Atlantic Multidecadal Oscillation. *J. Climate*, 21(11), 2371-2383.

Jiang, X. Y. and Z. L. Yang, 2012: Projected changes of temperature and precipitation in Texas from downscaled global climate models, *Clim. Res.*, 53,229-244.

636 Kalnay, E., M. Kanamitsu, R. Kistler , W. Collins, D. Deaven, L. Gandin, M. Iredell, S. Saha, G.
637 White, J. Woollen, Y. Zhu, M. Chelliah, W. Ebisuzaki, W. Higgins, J. Janowiak, K. Mo,
638 C. Ropelewski, J. Wang, A. Leetma, R. Reynolds, R. Jenne, and D. Joseph, 1996: The
639 NCEP-NCAR 40-Year Reanalysis Project. *Bull. Amer. Meteor. Soc*., 77, 437–471.
640
641 Karl, T. R., J.M. Melillo, T.C. Peterson, D.M. Anderson, D.F. Boesch, V. Burkett, L.M. Carter,
642 S.J. Cohen, N.B. Grimm, J.L. Hatfield, K. Hayhoe, A. Janetos, J.A. Kaye, J. Lawrimore,
643 J. McCarthy, A.D. McGuire, E. Miles, E. Mills, J.T. Overpeck, J. Patz, R. Pulwarthy, B.
644 Santer, M.J. Savonis, H.G. Schwartz, E. Shea, J. Stone, B.H. Udall, J. Walsh, M.F.
645 Wehner, T.J. Wilbanks, and D. Wuebbles. , 2009: *Global Climate Change Impacts in the*
646 *United States: A State of Knowledge Report from the U.S. Global Change Research*
647 *Program.* Cambridge University Press.
648
649 Kistler, R. et al. 2001: The NCEP-NCAr 50-Year reanalysis: Monthly means CD-ROM and
650 documentation, *Bull. Amer. Met. Soc.* 28, 2, 247-267.
651
652 Kushnir, Y., R. Seager, M. F. Ting, N. Naik, and J. Nakamura, 2010: Mechanisms of Tropical
653 Atlantic SST Influence on North American Precipitation Variability. *Journal of Climate*,
654 23, 5610-5628.
655
656 Li, W. H., R. Fu, R. I. N. Juarez, and K. Fernandes, 2008: Observed change of the standardized
657 precipitation index, its potential cause and implications to future climate change in the
658 Amazon region. *Philosophical Transactions of the Royal Society B-Biological Sciences*,
659 363, 1767-1772.
660
661 Li, W. H., L. F. Li, R. Fu, Y. Deng, and H. Wang, 2011: Changes to the North Atlantic
662 Subtropical High and Its Role in the Intensification of Summer Rainfall Variability in the
663 Southeastern United States. *Journal of Climate*, 24, 1499-1506.
664
665 Madden, R., and J. Williams, 1978: The correlation between temperature and 1071 precipitation
666 in the United States and Europe. *Mon. Wea. Rev*., 106, 142-147.
667
668 McCabe, G. J., M. A. Palecki, and J. L. Betancourt, 2004: Pacific and Atlantic Ocean influences
669 on multidecadal drought frequency in the United States. *Proceedings of the National*
670 *Academy of Sciences of the United States of America*, 101, 4136-4141.
671
672 McKee, T. B., N.J. Doesken, N.J., J. Kleist. , 1993: The relationship of drought frequency and
673 duration to time scales. *Eighth Conference on Applied Climatology*.
674
675 Meehl, G. A., C. Covey, T. L. Delworth, M. Latif, B. McAveney, J. F. B. Mitchell, R. J.
676 Stouffer, and K. E. Taylor, 2007b: The WCRP CMIP3 multimodel dataset: A new era in
677 climate change research. *Bull. Amer. Meteor. Soc.*, 88, doi:10.1175/BAMS-88-9-1383
678
679 Mishra, A. K. and V. P. Singh, 2009: Analysis of drought severity-area-frequency curves using a
680 general circulation model and scenario uncertainty, *J. Geophy. Res.* 114, D06120, 18 PP.,
681 doi:10.1029/2008JD010986

Mo, K. C., 2010: Interdecadal Modulation of the Impact of ENSO on Precipitation and Temperature over the United States. *Journal of Climate*, 23, 3639-3656.

Mo, K. C., J. K. E. Schemm, and S. H. Yoo, 2009: Influence of ENSO and the Atlantic Multidecadal Oscillation on Drought over the United States. *Journal of Climate*, 22, 5962-5982.

Moss, R. H., J. A. Edmonds, K. A. Hibbard, M. R. Manning, S. K. Rose, D. P. van Vuuren, T. R. Carter, S. Emori, M. Kainuma, T. Kram, G. A. Meehl, J. F. B. Mitchell, N. Nakicenovic, K. Riahi, S. J. Smith, R. J. Stouffer, A. M. Thomson, J. P. Weyant and T. J. Wilbanks, 2010: The next generation of scenarios for climate change research and assessment. *Nature*, 463, doi:10.1038/nature08823.

Myoung, B. and Nielsen-Gammon, J. W. (2010). The Convective Instability Pathway to Warm Season Drought in Texas. Part I: The Role of Convective Inhibition and Its Modulation by Soil Moisture. *Journal of Climate*, 23(17): 4461-4473

Nigam, S., B. Guan, and A. Ruiz-Barradas, 2011: Key role of the Atlantic Multidecadal Oscillation in 20th century drought and wet periods over the Great Plains. *Geophysical Research Letters*, 38.

O'Lenic, E. A., and Livezey, R.E. (1988), Practical considerations in the use of Rotated Principal Component Analysis (RPCA) in diagnostic studies of upper-air height fields, *Monthly Weather Review*, *116*, 1682-1689.

Pierce, D. W., T. P. Barnett, B. D. Santer, and P. J. Gleckler (2009), Selecting global climate models for regional climate change studies, *Proc. National Academy of Sciences*, *106*(21), 8441-8446.

Richman, M. B. (1987), Rotation of principal components: a reply, *Journal of Climatology*, *7*, 511-520.

Rodell, M., and Coauthors, 2004: The global land data assimilation system. *Bulletin of the American Meteorological Society*, 85, 381-393.

Schubert, S, D. Gutzler, H. L. Wang, A. Dai, T. Delworth, C. Deser, K. Findell, **R. Fu**, W. Higgins, M. Hoerling, B. Kirtman, R. Koster, A. Kumar, D. Legler, D. Lettenmaier, B. Lyon[1] V. Magana, K. S. Mo, S. Nigam, P. Pegion, A. Phillips, R. Pulwarty, D. Rind, A. Ruiz-Barradas, J. Schemm, R. Seager, R. Stewart, M. Suarez, J. Syktus, M.F. Ting, C.Z. Wang, S. Weaver, N. Zeng, 2009: A USCLIVAR Project to Assess and Compare the Responses of Global Climate Models to Drought-Related SST Forcing Patterns: Overview and Results, *J. Climate*, 22, 5251-5272.

Seager, R, M. F. Ting, I. Held, Y. Kushnir, J. Lu, G Vecchi, H. P. Huang, N. Harnik, A. Leetmaa, N. C. Lau, C. h. Li, J. Velez, N. Naik-2007: Model Projections of an Imminent Transition to a More Arid Climate in Southwestern North America, *Science*, 316, 1181-

1184. DOI: 10.1126/science.1139601

Smith, T. M., R. W. Reynolds, T. C. Peterson, and J. Lawrimore, 2008: Improvements to NOAA's historical merged land-ocean surface temperature analysis (1880-2006). *Journal of Climate*, 21, 2283-2296.

Stevenson, S. L., 2012: Changes to ENSO strength and impacts in the CMIP5 models. *JGR*, In press.

Taylor K.E. (2001) Summarizing multiple aspects of model performance in a single diagram. *J Geophys Res* 106(D7):7183-7192. doi:10.1029/2000jd900719

Trenberth, K. E., P.D. Jones, P. Ambenje, R. Bojariu, D. Easterling, A. Klein Tank, D. Parker, F. Rahimzadeh, J.A. Renwick, M. Rusticucci, B. Soden and P. Zhai, 2007: Observations: Surface and Atmospheric Climate Change. In: Climate Change 2007: The Physical Science Basis. *Contribution of Working Group I to the Fourth Assessment Report of the Intergovernmental Panel on Climate Change* [Solomon, S., D. Qin, M. Manning, Z. Chen, M. Marquis, K.B. Averyt, M. Tignor and H.L. Miller (eds.)].

Vose, R. S , T. C. Peterson, R. L. Schmoyer, J. K. Eischeid, P. M. Steurer, R. R. Heim and T. R., Karl, 1993. The GlobalHistorical Climatology Network: Long-term monthly temperature, precipitation, and pressure data. *Fourth AMS Symposium on Global Change Studies,* Anaheim, CA., January 17-22 1993.

Wang, H., R. Fu, A. Kumar, and W. H. Li, 2010: Intensification of Summer Rainfall Variability in the Southeastern United States during Recent Decades. *Journal of Hydrometeorology*, 11, 1007-1018.

Weiss, J. L., C. L. Castro, and J. T. Overpeck, 2009: Distinguishing Pronounced Droughts in the Southwestern United States: Seasonality and Effects of Warmer Temperatures. *Journal of Climate*, 22, 5918-5932.

Wittengberg, A. T., 2009: Are historical records sufficient to constrain ENSO simulations? GRL, 36, L12702, doi:10.1029/2009GL038710.

Wu, R. G., and J. L. Kinter, 2009: Analysis of the Relationship of US Droughts with SST and Soil Moisture: Distinguishing the Time Scale of Droughts. *Journal of Climate*, 22, 4520-4538.

Yeh, S. W., J. S. Kug, B. Dewitte, M. H. Kwon, B. P. Kirtman & F. F. Jin**,** 2009**:** El Niño in a changing climate, *Nature*, 461, 511–514, doi:10.1038/nature08316.

Figure Captions:

Fig. 1: Spatial domain of the SC US defined in this study.

Fig. 2: Seasonal cycles of daily maximum and minimum surface temperature (Tmax, Tmin) and specific humidity (qsfc) derived from observations and historical simulations of the CMIP5 models for the period of 1950-2005. The numbers in the parentheses are the model ensembles.

Fig. 3: As in Fig. 2 but for seasonal cycles of precipitation (P), evapotranspiration (ET) and the net downward water flux (P-ET).

Fig. 4: Observed and modeled PDF of Tmax (top), Tmin (middle) and rainrate (bottom), and PDF of modeled minus observed rainrate for each model for the period of 1950-2005. One ensemble member from each model is used.

Fig. 5: Box plots comparing observed and modeled SPI6 and SPI9 derived from historical simulations of the CMIP5 models. The red lines at the centers of the boxes represent the median of the SPI values, whereas the upper and lower ends of the boxes represent 75% and 25% levels of the SPI values. Red crosses represent the outliners of the SPI values.

Fig. 6: Comparison of the modeled Z500hPa pattern by each of the CMIP5 models with that of NCEP-CDAS1.

Fig. 7: As in Fig. 6, but for U850.

Fig. 8: As in Fig. 6, but for V850.

Fig. 9: Correlations between Niño4, Niño3 and the SC US rainfall. "Star" indicates significant correlation coefficient at 95% confidence level using the Student t-test.

Fig. 10: Correlation pattern between 500hPa geopotential anomalies and Niño3 index obtained from NCEP reanalysis and the historical simulations by the nine CMIP5 models for the period of 1979-2005.

Fig. 11: As in Fig. 10 but for correlation with the Niño4 index.

Fig. 12: Correlation coefficient between the SC US rainfall anomalies and AMO index. "Star" indicates significant correlation coefficient at 95% confidence level using the Student t-test.

Fig. 13: The leading mode of REOF (REOF1) derived from observed and modeled SSTA from the nine CMIP5 models.

Fig. 14: comparing linear regression between the SC US P and T with the warming modes between models and observations. "Circle" indicates significant correlation coefficient at 95% confidence level using the Student t-test.

Fig. 15: Projected changes of surface daily maximum temperature during period of 2071-2100 under the RCP4.5 and RCP8.5 scenarios, compared to the historical simulations of the CMIP5 models and observation during the period of 1979-2005.

Fig. 16: As in Fig. 15 but for Tmin.

Fig. 17: Projected changes of rainrate distribution between the period of 2071-2100 and that of 1979-2005 for the RCP4.5 (red) and RCP8.5 (blue) scenarios for the nine CMIP5 models.

Fig. 19: Projected SPI6 over the SC US based on projected rainfall for the period of 2071-2100 for the RCP4.5 and RCP8.5 scenario, respectively, and rainfall climatology and variability from the historical simulations for the period of 1979-2005.

836 Table 1. Description of CMIP5 models used in this study

Model (Fig marker)	Institute (Country)	Available Ensembles	Components (Resolutions)	Calendar	Reference
CCSM4 (A)	National Center for Atmospheric Research (USA)	6	F09_g16 (0.9×1.25_gx1v6)	No leap	Gent et al., 2011
GFDL-ESM2M (B)	NOAA/Geophysical Fluid Dynamics Laboratory (USA)	1	Atm: AM2 (AM2p14, M45L24) Ocn: MOM4.1 (1.0° lat ×1.0° lon, enhanced tropical resolution: 1/3 on the equator)	No leap	John Dunne et al., 2012
GFDL-ESM2G (C)	NOAA/Geophysical Fluid Dynamics Laboratory (USA)	1	Atm: AM2 (AM2p14, M45L24) Ocn: MOM4.1 (1.0° lat ×1.0° lon, enhanced tropical resolution: 1/3 on the equator)	No leap	John Dunne et al., 2012
GISS-E2-R (D)	NASA/Goddard Institute for Space Studies (USA)	5	Atm: GISS-E2 (2.0° lat ×2.5° lon) Ocn: R	No leap	Schmidt et al., 2006
HadGEM2-CC (E)	Met Office Hadley Centre (UK)	3	Atm: HadGAM2 (N96L60) Ocn: HadGOM2 (Lat: 1.0-0.3 Lon: 1.0 L40)	360 d/y	Collins et al., 2011; Martin et al., 2011
MPI-ESM-LR (F)	Max Planck Institute for Meteorology (Germany)	3	Atm: ECHAM6 (T63L47) Ocn: MPIOM (GR15L40)	Gregorian	Raddatz et al., 2007; Marsland et al., 2003
IPSL-CM5A-LR (G)	Institut Pierre Simon Laplace (France)	5	Atm: LMDZ4 (96×95×39, 1.875° lat ×3.75° lon) Ocn: ORCA2 (2×2L31, 2.0° lat ×2.0° lon)	No leap	Marti et al., 2010
MIROC5 (H)	AORI, NIES & JAMSTEC (Japan)	4	Atm: AGCM6 (T85L40) Ocn: COCO (COCO4.5)	No leap	Watanabe et al., 2010
MRI-CGCM3 (I)	Meteorological Research Institute (Japan)	3	Atm: GSMUV (TL159L48) Ocn: COM3 (1×0.5L51)	Gregorian	Yukimoto et al., 2011

837

838 Table 2: Ranking of model performance for SC US regional climate change

Variables	*Models*								
	CCSM4	GFDL-ESM2G	GFDL-ESM2M	GISS-E2-R	HadGEM2	MPI	IPSL	MIROC5	MRI
					Correlation with global SST warming:				
a_{GW}	1	3	1	3	2	3	3	3	3
GW_{SST}	2	1	3	1	3	2	2	3	2
Subtotal	1.5	2	2	2	2.5	2.5	2.5	3	2.5
					Seasonal cycle:				
Tmax	1	2	2	2	1	2	3	1	2
Tmin	2	1	1	1	3	1	3	2	1
q	1	1	2	1	3	1	3	1	1
Subtotal	1.3	1.3	1.7	1.3	2.3	1.3	3	1.3	1.3
PD_{Tmax}	3	3	3	3	3	3	3	3	2
PD_{RR}	2	2	2	2	2	2	2	2	1
P	1	3	3	2	3	1	2	2	3
ET	3	2	2	3	2	2	2	2	2
SPI6	2	2	2	2	2	2	2	2	2
SPI9	2	2	2	2	2	2	2	2	2
Subtotal	2.2	2.3	2.3	2.3	2.3	2	2.2	2.2	2
Z500	2	3	3	3	2	2	3	2	3
U850	1	2	2	2	2	1	1	2	2
V850	2	2	2	2	1	2	2	2	2
Subtotal	1.7	2.3	2.3	2.3	1.7	1.7	2	2	2.3
					Natural variability				
$r_{p,Niño3}$	3	2	2	1	3	3	3	2	3
SZ500, Niño3	2	2	2	3	3	3	3	3	3
$r_{p,Niño4}$	3	2	2	1	3	3	3	2	3
SZ500, Niño4	2	2	2	3	3	3	3	2	3
Subtotal	2.5	2	2	2	3	3	3	2.3	3

839
840 Ranking 1: Generally realistic pattern, Ranking 2: partially realistic, Ranking 3: No resemblance to those observed
841 α_{GW}: Linear regression coefficient between SC US summer rainfall anomalies and PC of the global SST warming
842 mode of the REOF analysis of global SST anomalies for the period of 1950-2005; GW_{SST}: Spatial pattern of the
843 global SST warming mod; PD_{Tmax}: Probability distribution of daily maximum surface temperature. PD_{RR}:
844 Probability distribution of rainrate; $r_{p,Niño3}$, $r_{p,Niño4}$: Correlation coefficient between SC US rainfall anomalies and
845 Niño3 index and Niño4 index, respectively; SZ500, Niño3, SZ500, Niño4: Spatial patterns of the regression between
846 Z500 anomalies and Niño3 index and Niño4 index, respectively.
847
848
849

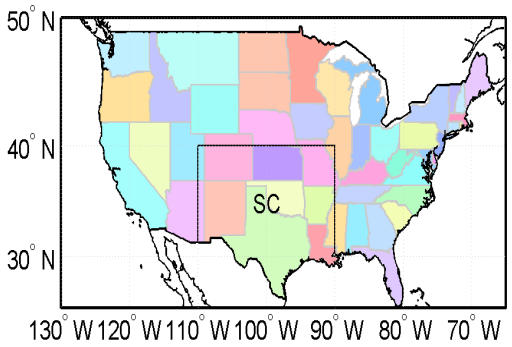

Fig. 1: Spatial domain of the SC US defined in this study.

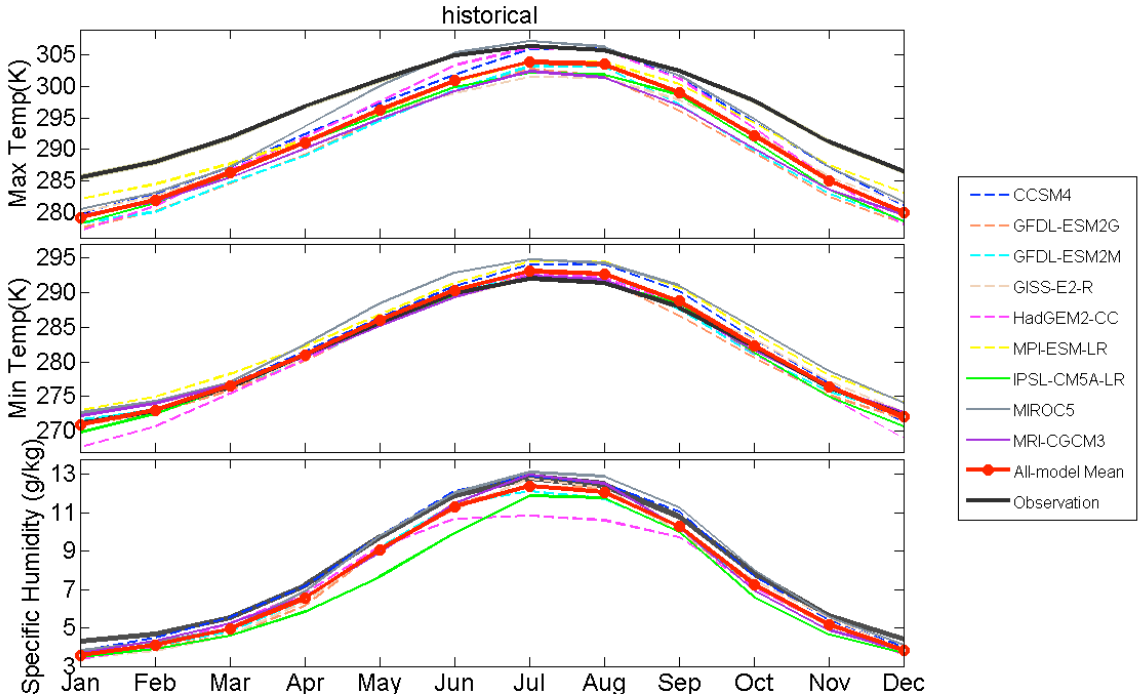

Fig. 2: Seasonal cycles of daily maximum and minimum surface temperature (Tmax, Tmin) and specific humidity (qsfc) derived from observations and historical simulations of the CMIP5 models for the period of 1950-2005. The numbers in the parentheses are the model ensembles.

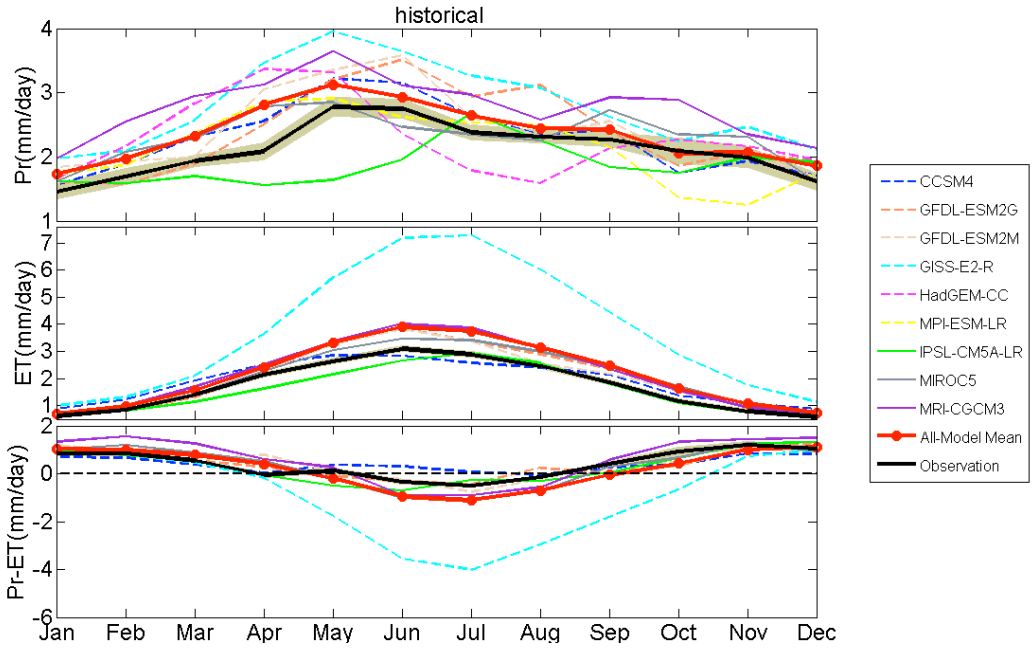

Fig. 3: As in Fig. 2 but for seasonal cycles of precipitation (P), evapotranspiration (ET) and the net downward water flux (P-ET).

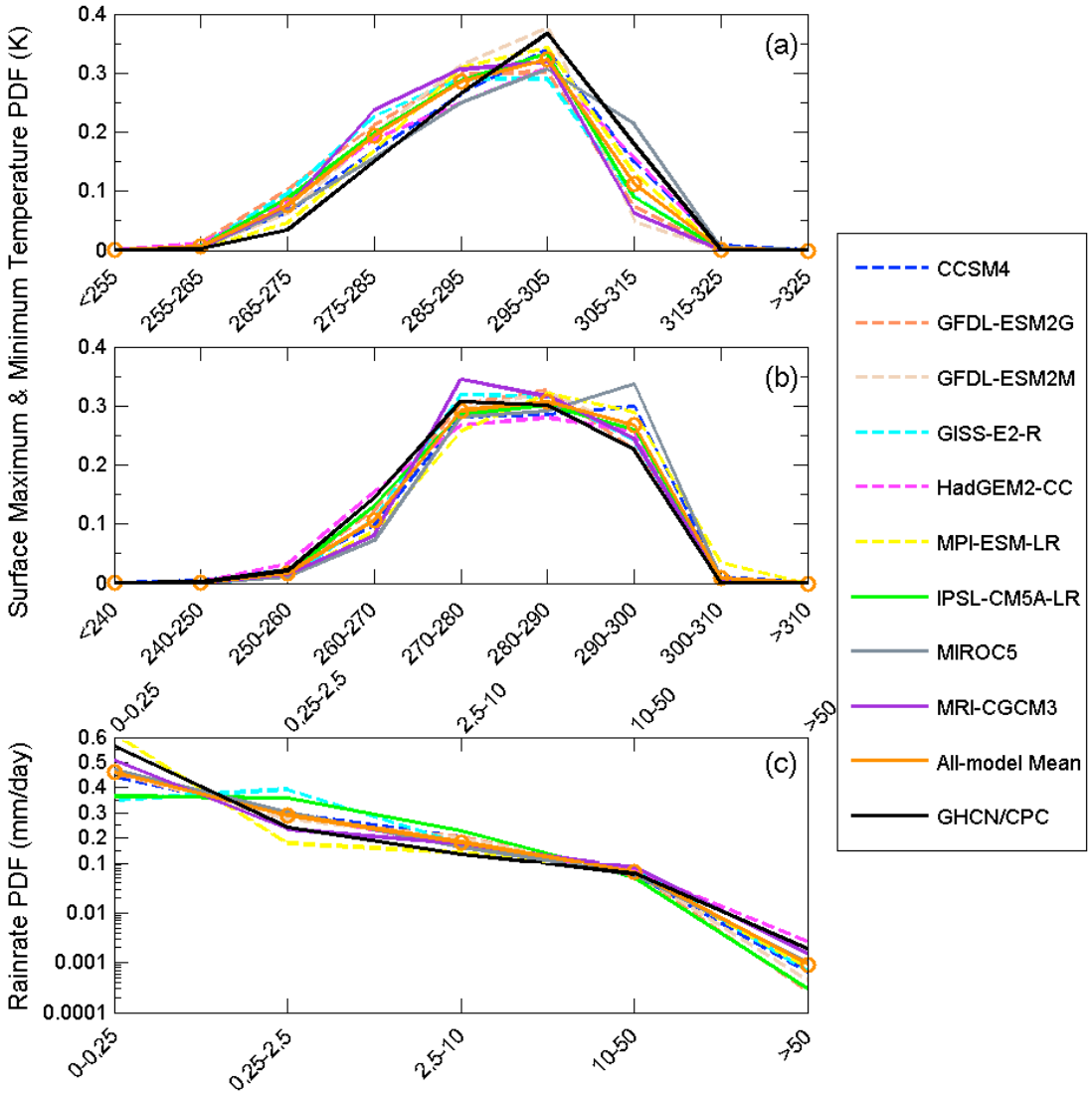

Fig. 4: Observed and modeled PDF of Tmax (top), Tmin (middle) and rainrate (bottom), and PDF of modeled minus observed rainrate for each model for the period of 1950-2005. One ensemble member from each model is used.

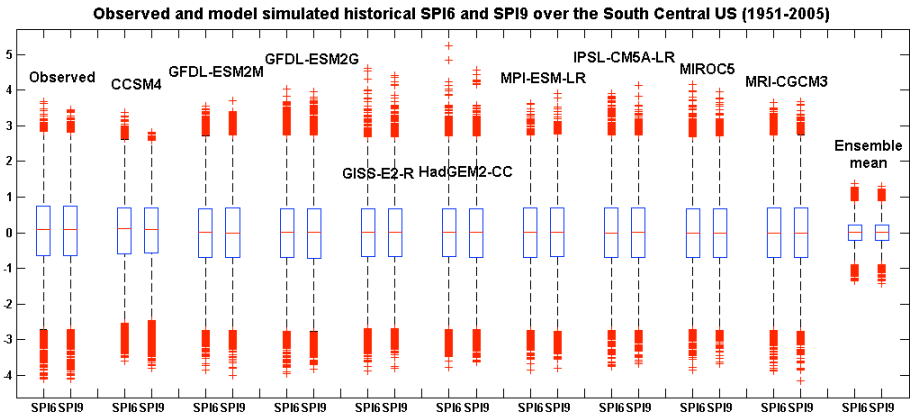

Fig. 5: Box plots comparing observed and modeled SPI6 and SPI9 derived from historical simulations of the CMIP5 models. The red lines at the centers of the boxes represent the median of the SPI values, whereas the upper and lower ends of the boxes represent 75% and 25% levels of the SPI values. Red crosses represent the outliners of the SPI values.

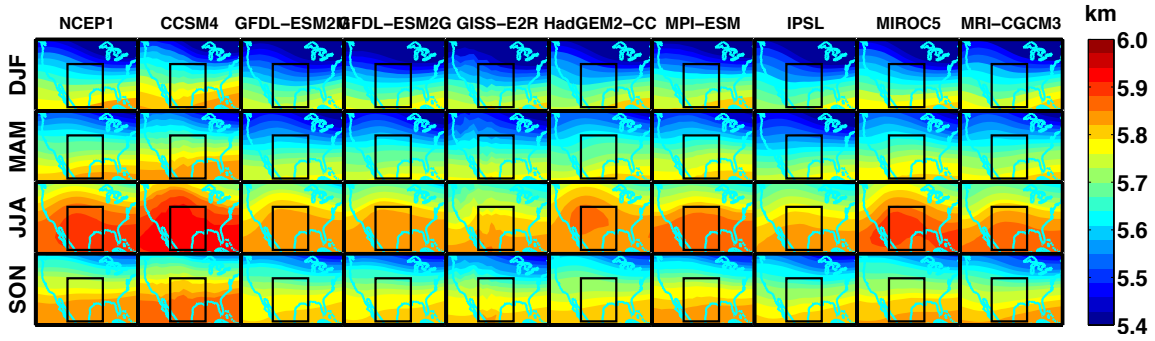

Fig. 6: Comparison of the modeled Z500hPa pattern by each of the CMIP5 models with that of NCEP-CDAS1.

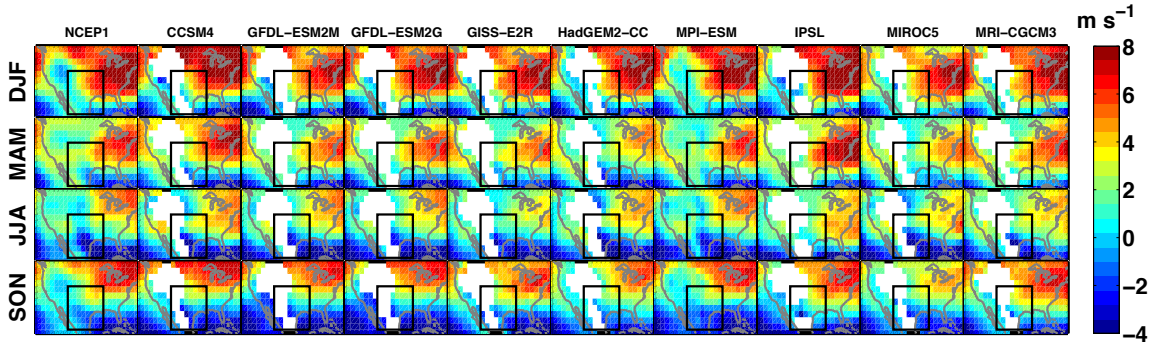

Fig. 7: As in Fig. 6, but for U850.

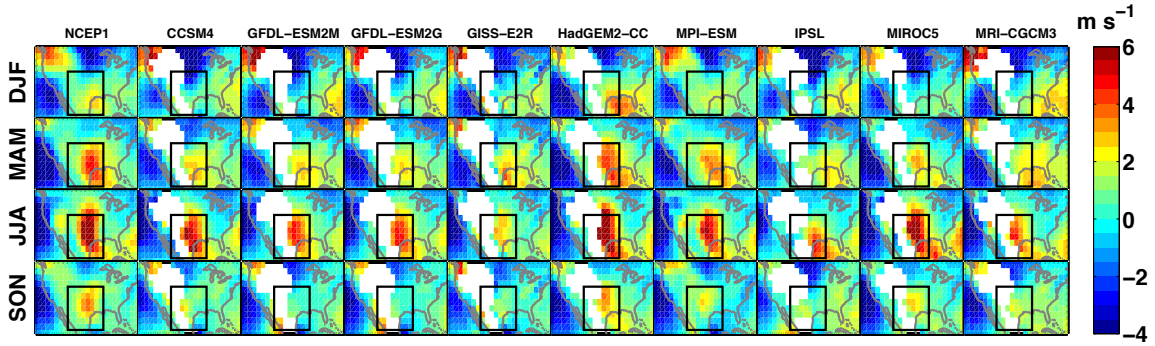

Fig. 8: As in Fig. 6, but for V850.

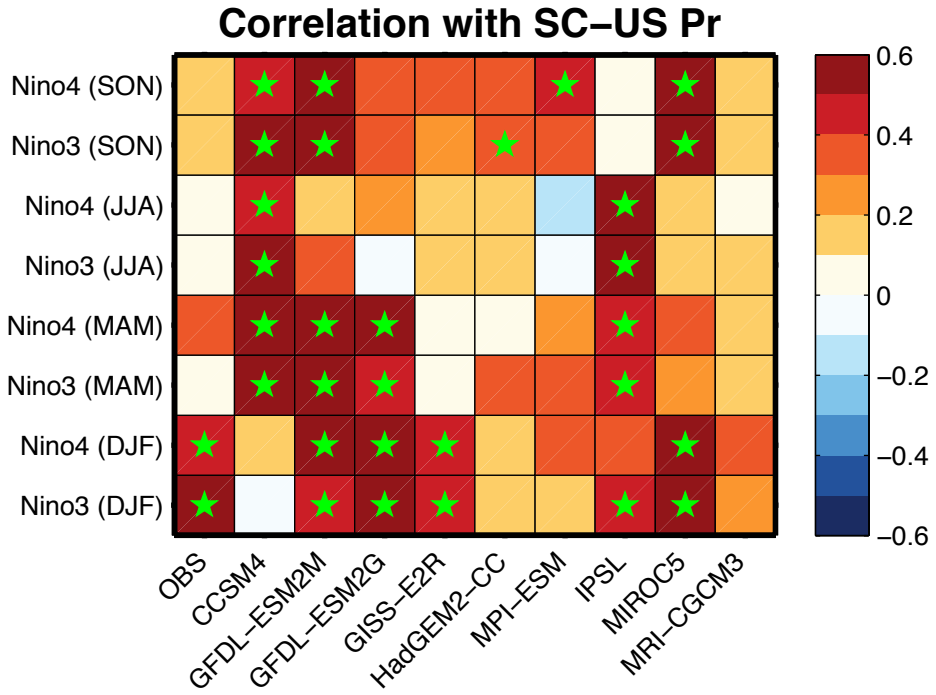

Fig. 9: Correlations between Niño4, Niño3 and the SC US rainfall. "Star" indicates significant correlation coefficient at 95% confidence level using the Student t-test.

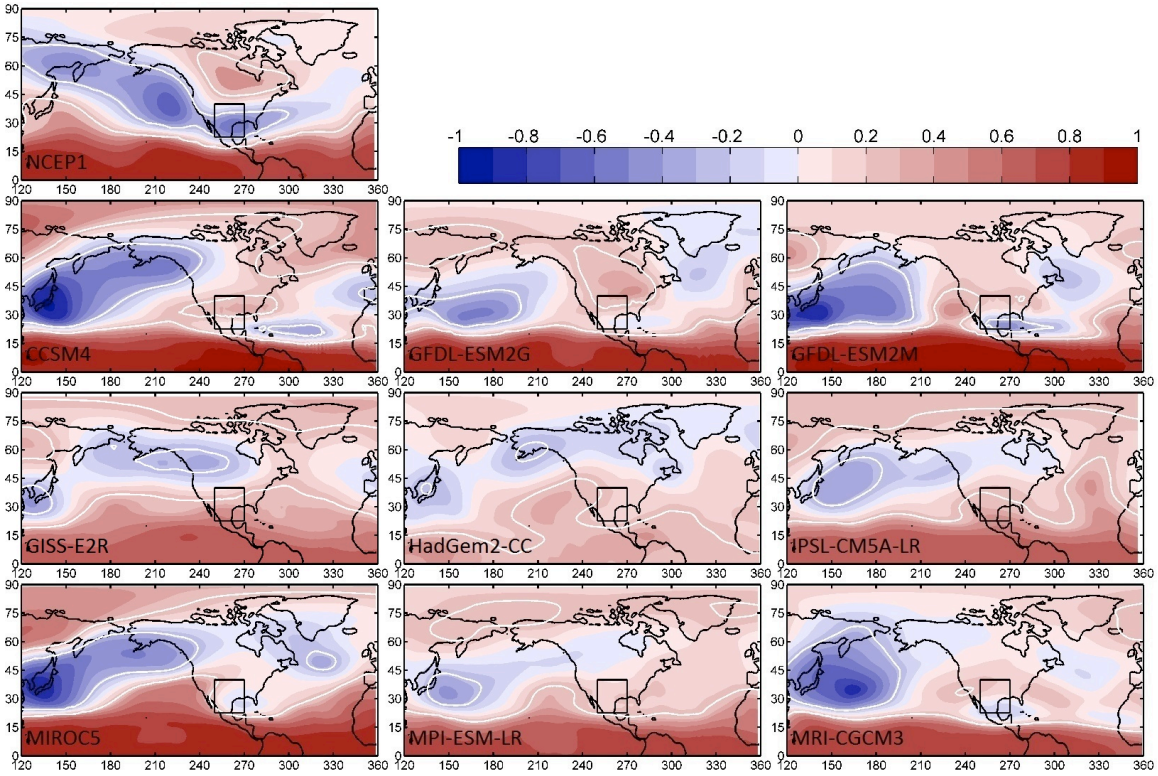

Fig. 10: Correlation pattern between 500hPa geopotential anomalies and Niño3 index obtained from NCEP reanalysis and the historical simulations by the nine CMIP5 models for the period of 1979-2005.

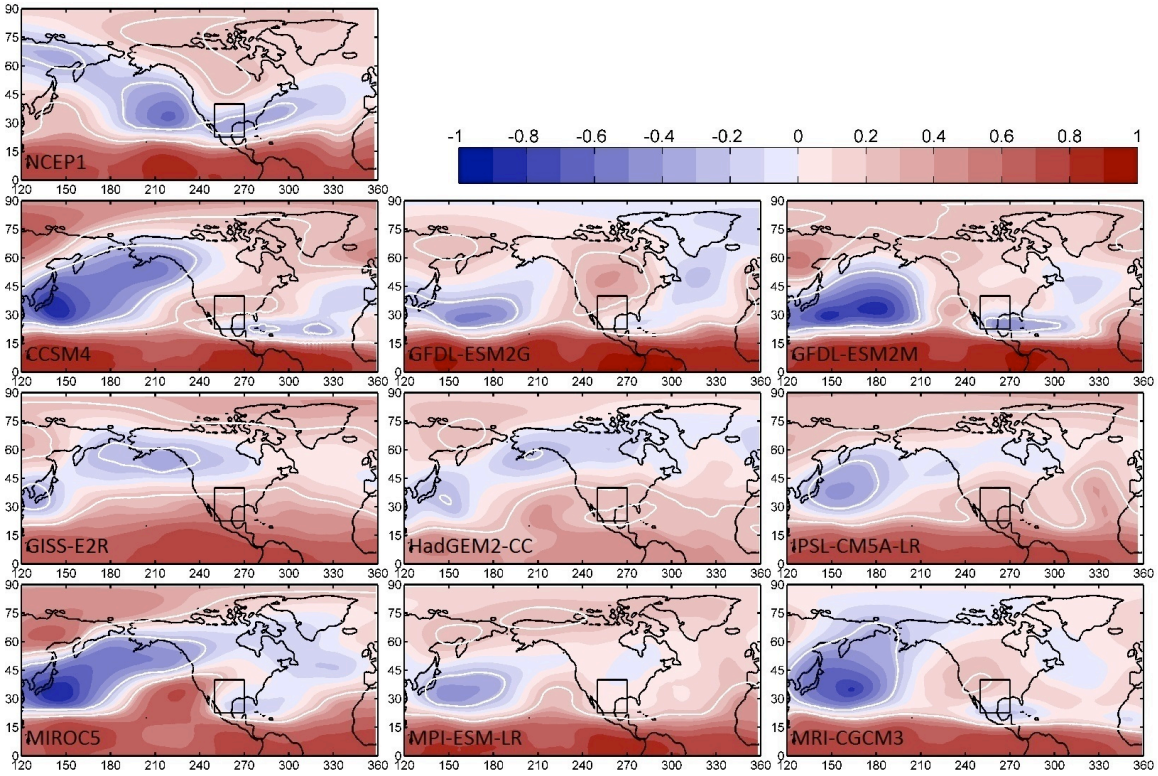

Fig. 11: As in Fig. 10 but for correlation with the Niño4 index.

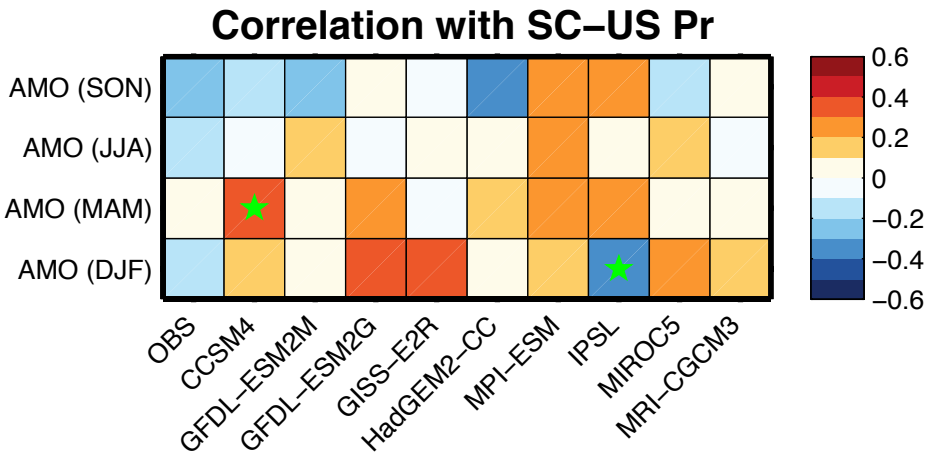

Fig. 12: Correlation coefficient between the SC US rainfall anomalies and AMO index. "Star" indicates significant correlation coefficient at 95% confidence level using the Student t-test.

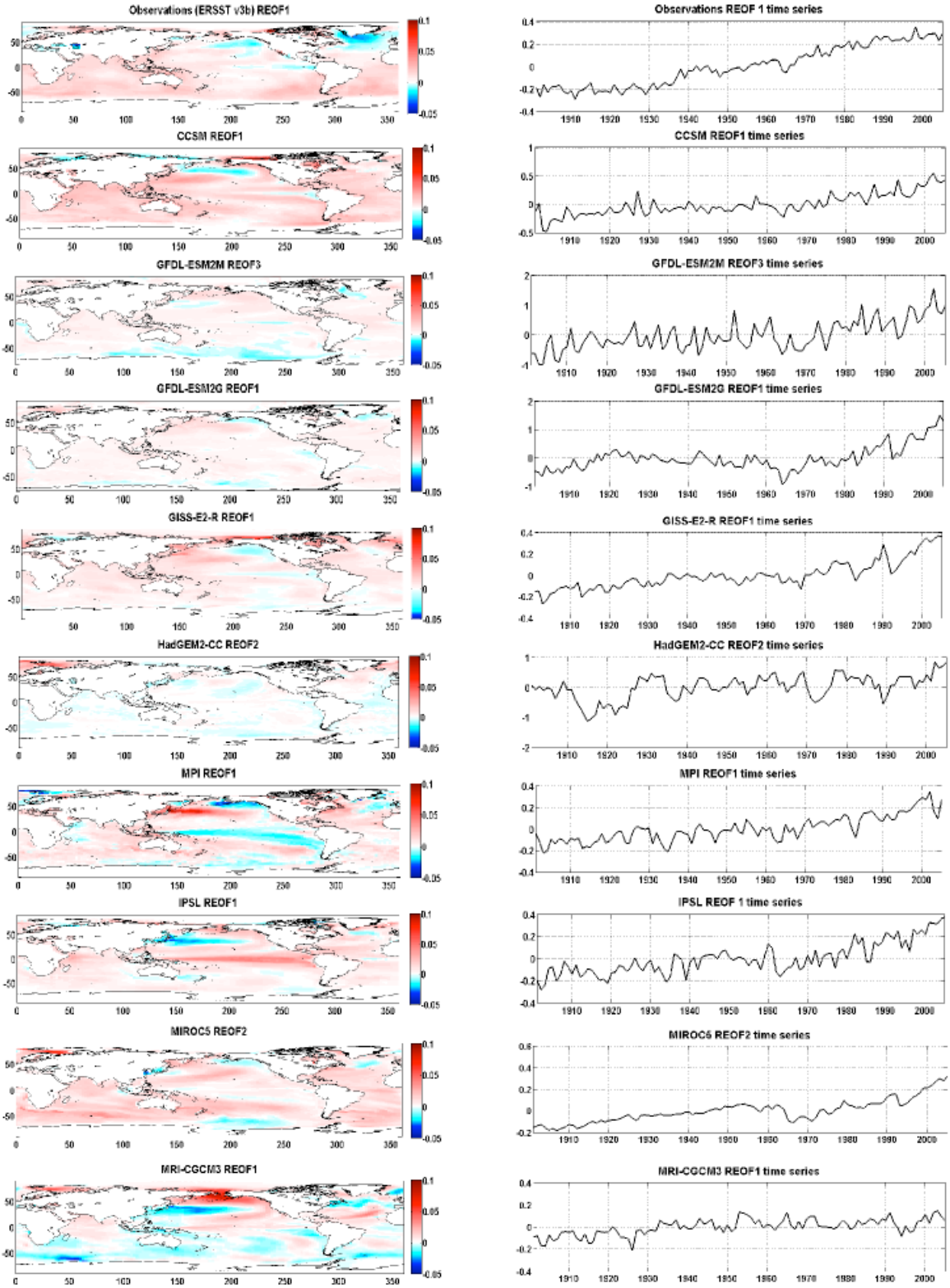

Fig. 13: The leading mode of REOF (REOF1) derived from observed and modeled SSTA from the nine CMIP5 models.

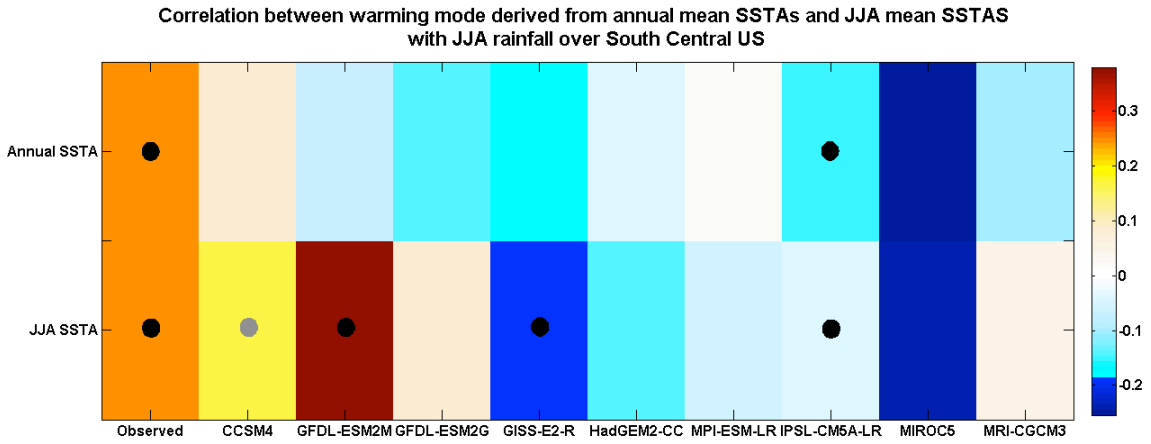

Fig. 14: comparing linear regression between the SC US P and T with the warming modes between models and observations. "Circle" indicates significant correlation coefficient at 95% confidence level using the Student t-test.

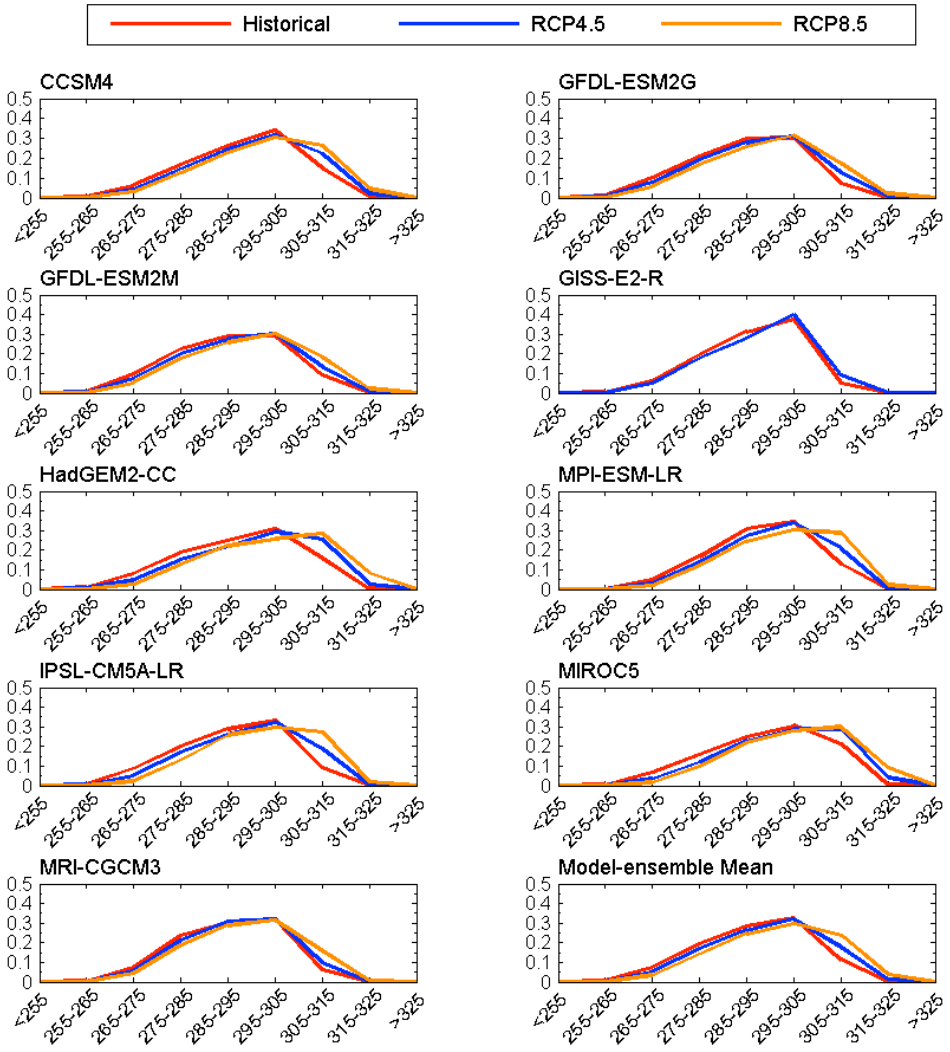

Fig. 15: Projected changes of surface daily maximum temperature during period of 2071-2100 under the RCP4.5 and RCP8.5 scenarios, compared to the historical simulations of the CMIP5 models and observation during the period of 1979-2005.

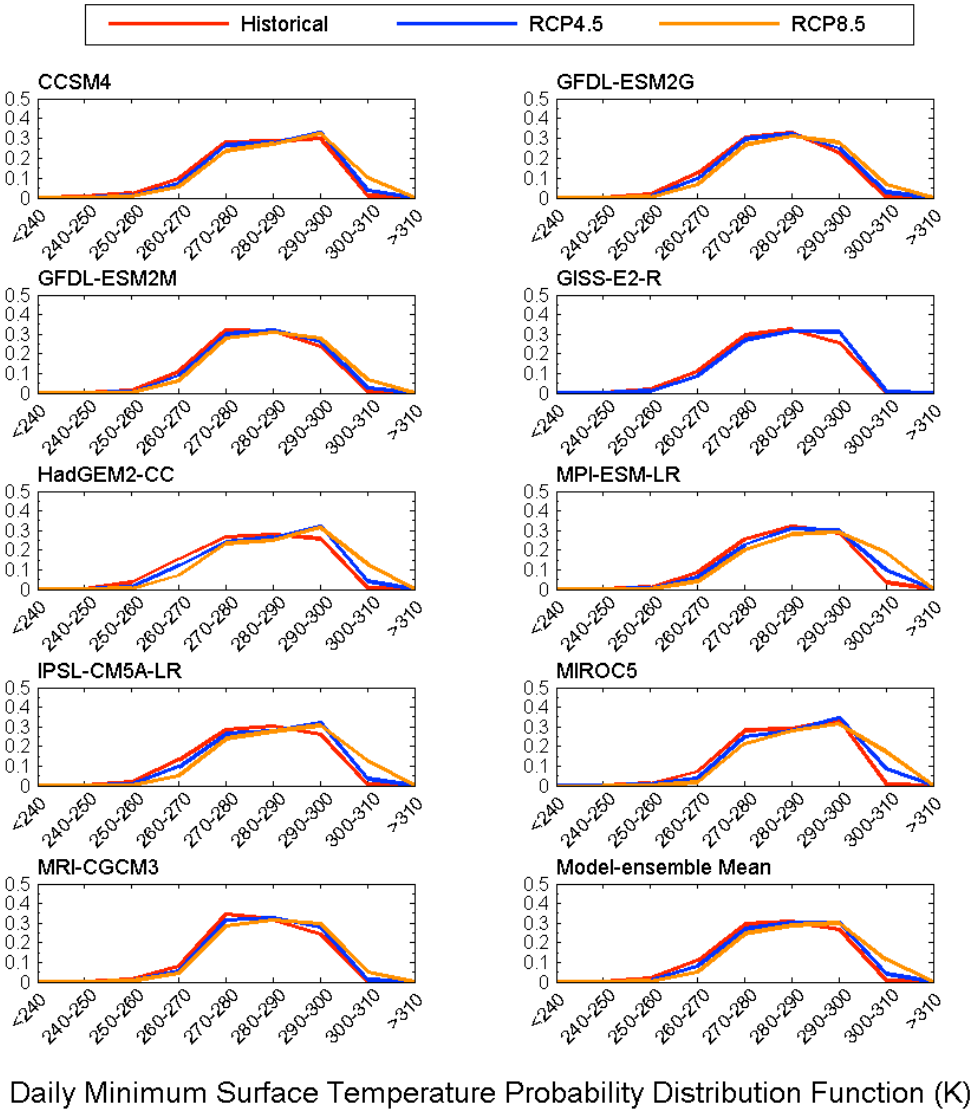

Fig. 16: As in Fig. 15 but for Tmin.

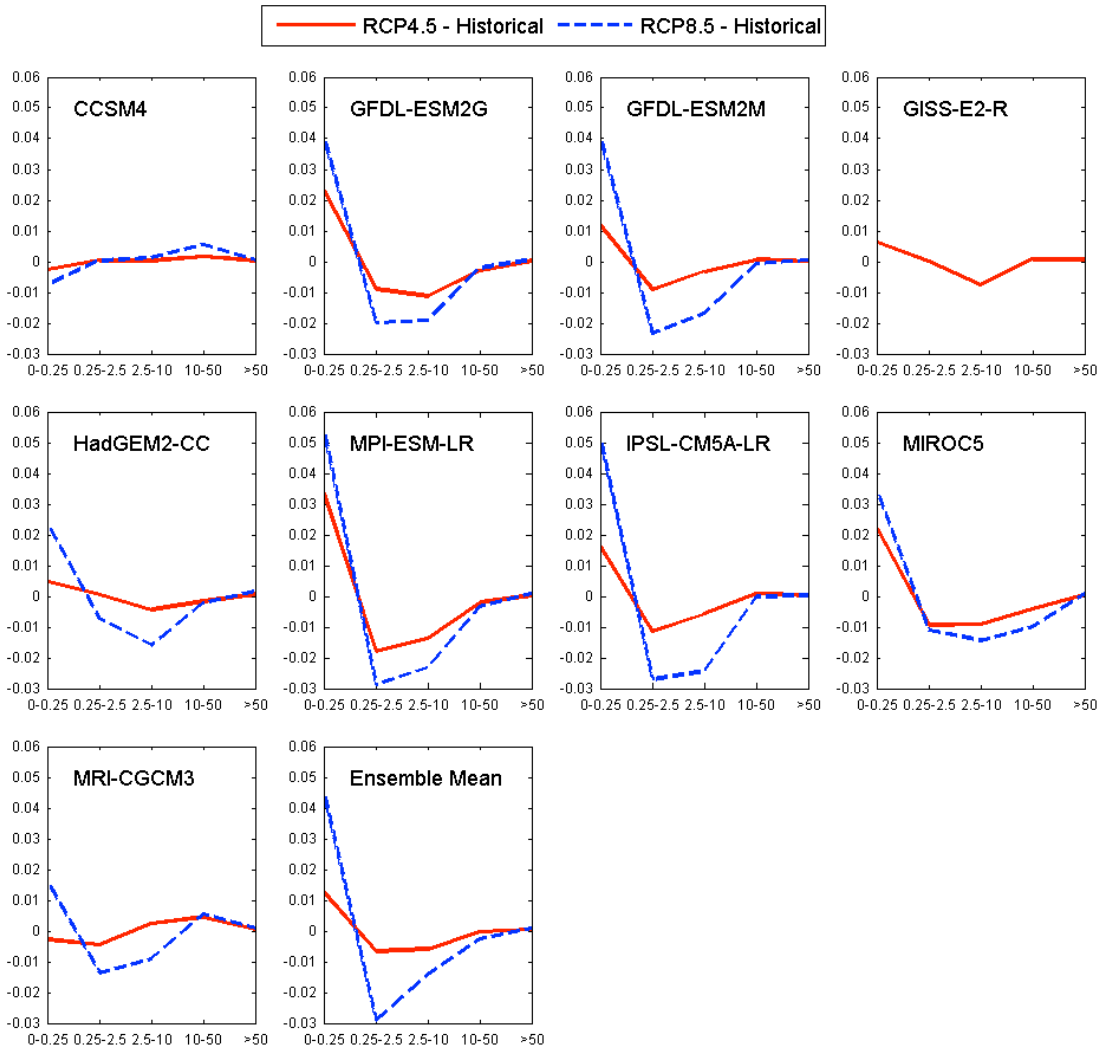

Fig. 17: Projected changes of rainrate distribution between the period of 2071-2100 and that of 1979-2005 for the RCP4.5 (red) and RCP8.5 (blue) scenarios for the nine CMIP5 models.

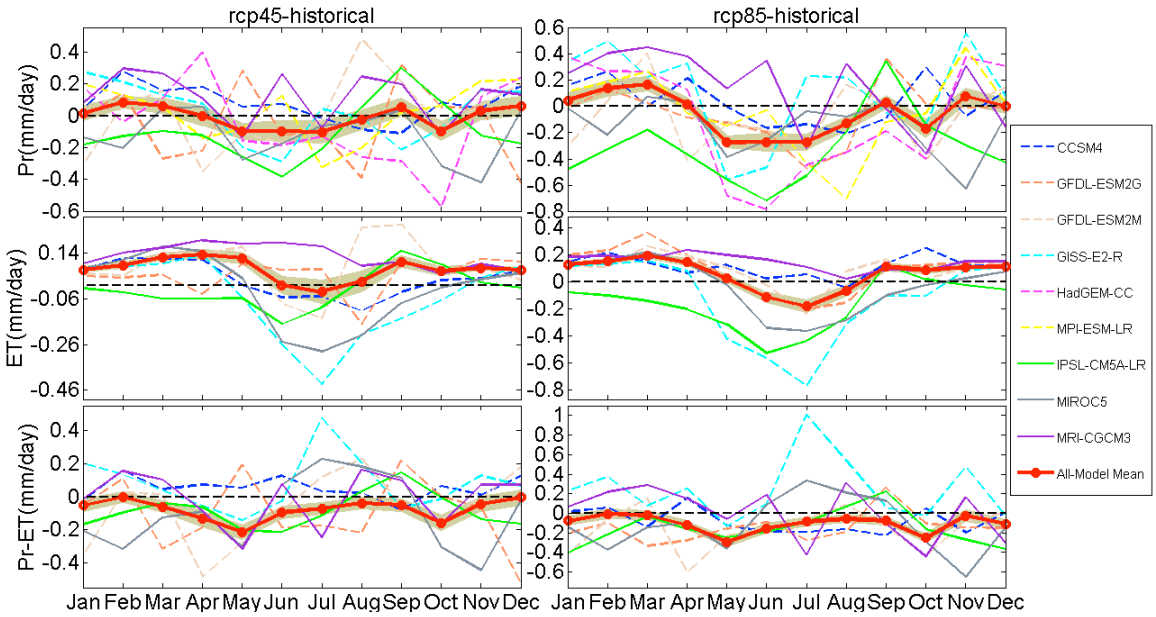

Fig. 18: Changes of climatological seasonal cycles of P, ET and P-ET between the period of 2071-2100 for the RCP4.5 and RCP8.5 scenarios and those from the historical simulations for the period of 1979-2005.

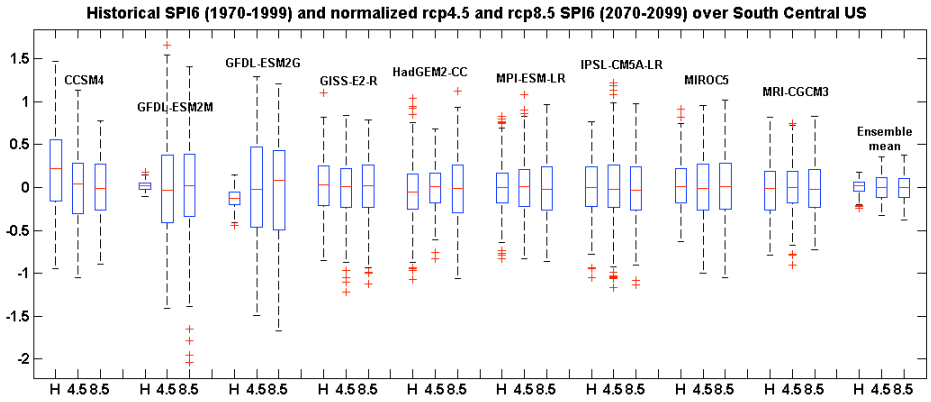

Fig. 19: Projected SPI6 over the SC US based on projected rainfall for the period of 2071-2100 for the RCP4.5 and RCP8.5 scenario, respectively, and rainfall climatology and variability from the historical simulations for the period of 1979-2005.